Ecological Monographs, 84(1), 2014, pp. 109–129

Carbon transit through degradation networks

David C. Forney[1,2,3] and Daniel H. Rothman[1]

[1]*Lorenz Center and Department of Earth, Atmospheric, and Planetary Sciences, Massachusetts Institute of Technology, Cambridge, Massachusetts 02139 USA*
[2]*Department of Mechanical Engineering, Massachusetts Institute of Technology, Cambridge, Massachusetts 02139 USA*

Abstract. The decay of organic matter in natural ecosystems is controlled by a network of biologically, physically, and chemically driven processes. Decomposing organic matter is often described as a continuum that transforms and degrades over a wide range of rates, but it is difficult to quantify this heterogeneity in models. Most models of carbon degradation consider a network of only a few organic matter states that transform homogeneously at a single rate. These models may fail to capture the range of residence times of carbon in the soil organic matter continuum. Here we assume that organic matter is distributed among a continuous network of states that transform with stochastic, heterogeneous kinetics. We pose and solve an inverse problem in order to identify the rates of carbon exiting the underlying degradation network (exit rates) and apply this approach to plant matter decay throughout North America. This approach provides estimates of carbon retention in the network without knowing the details of underlying state transformations. We find that the exit rates are approximately lognormal, suggesting that carbon flow through a complex degradation network can be described with just a few parameters. These results indicate that the serial and feedback processes in natural degradation networks can be well approximated by a continuum of parallel decay rates.

Key words: carbon cycle; carbon degradation; decomposition; litter; microbial decay networks; plant matter decay; soil organic carbon.

Introduction

The retention of particles in networks is associated with problems in ecosystems modeling (van Veen et al. 1984, Parton et al. 1987, 1993, Jenkinson et al. 1990, Sierra et al. 2011), drug kinetics (Faddy 1993, Matis and Wehrly 1998, 1990), logistics (Kendall 1953), industrial processing (Forrester 1961), and other fields (Godfrey 1983). Flow diagrams (Forrester 1961), Markov models (Matis and Wehrly 1990, Sierra et al. 2011), and compartmental models (Godfrey 1983) are used to model these networks, where information flows from one compartment to another in parallel, in series, or with feedback. Often, kinetic parameters and the general structures of these systems are unknown. These parameters can be identified by fitting model outputs to dynamic data. However when the underlying network structure (e.g., the number of pools/substrates, number of microbial species/communities and their connectivity) is unknown then identifying system parameters remains a challenge.

Here we investigate the retention of carbon in terrestrial organic matter. Plant litter is initially composed of many organic components that degrade at different rates (Tenney and Waksman 1929, Minderman 1968, Burdige 2006, Lutzow et al. 2006, Berg and McClaugherty 2007). As decomposition proceeds however, organic matter is transformed. Various kinds of extracellular enzymes break down polymers into shorter chains (Allison 2012, Sinsabaugh and Follstad Shah 2012), acids break free, and a diversity of decomposers transform compounds into decomposer biomass and other organic byproducts of the decomposition process. These compounds may then interact chemically (Lee et al. 2004, Berg and Laskowski 2006, Lützow et al. 2006), forming humic and other hard-to-degrade compounds degrade compounds (Eijsackers and Zehnder 1990, Berg and McClaugherty 2007, Paul 2007). Furthermore, particulate and dissolved carbon bond and sorb to clays and minerals (Oades 1988, Mayer 1994, Hedges and Oades 1997, Vetter et al. 1998, Nieder and Benbi 2008) forming organo-mineral complexes that also affect decomposability. In this manner, organic carbon is transformed from one pool to another by means of both serial and feedback processes.

Models of organic matter decomposition

The most commonly employed models of soil organic matter decomposition include these serial and feedback loops between various pools (van Veen et al. 1984, Parton et al. 1987, 1993, Jenkinson et al. 1990), but the network architecture is based purely on intuition about decomposer food chains and empirical results regarding the precursors for more recalcitrant soil organic matter.

Manuscript received 29 October 2012; revised 1 May 2013; accepted 7 May 2013. Corresponding Editor: A. T. Classen.
[3] Present address: EcoCorps, P.O. Box 235281, Encinitas, California 92023 USA. E-mail: forneyd@alum.mit.edu

Other models treat soil organic matter as a continuum, where transformations occur among a continuum of states (Bosatta 1985, Ågren and Bosatta 1998, Sierra et al. 2011). Recent degradation models include microbial community dynamics and degradation reactions catalyzed by extracellular enzyme concentrations (Schimel and Weintraub 2003, Manzoni and Porporato 2007, Allison 2012, Sinsabaugh and Follstad Shah 2012, Gangsheng et al. 2013). The most advanced of these models proceed in a manner consistent with the mechanisms described above: a community of microbe species expresses various extracellular enzymes, which degrade a variety of substrates. The enzymatic reactions in these models produce dissolved organic carbon monomers, some of which are anabolically converted to microbial biomass and some of which adsorb to soil clays (Gangsheng et al. 2013), becoming soil organic matter. Microbial biomass turns over and re-enters the organic carbon pool as an available substrate. Some models incorporate a spatial relationship between litter and community (Allison 2012), however most do not. By incorporating stoichiometric relationships between substrate and decomposer, these models also are able to couple the dynamics of nutrients such as nitrogen. These models, however, have some limitations. The kinetics of carbon degradation in these models relies exclusively on local concentrations of enzymes and Michaelis-Menten or Reverse Michaelis-Menten kinetics (Schimel and Weintraub 2003, Moorhead and Sinsabaugh 2006, Manzoni and Porporato 2007, Allison 2012, Sinsabaugh and Follstad Shah 2012, Gangsheng et al. 2013). Enzyme production and local enzymatic concentrations, however, are regulated (and limited) by a number of environmental chemical signals (Allison et al. 2011, Sinsabaugh and Follstad Shah 2012); yet the signal pathways and dynamics of relevant environmental input signals are not included in the models (Sinsabaugh and Follstad Shah 2012). Furthermore, there is a cascade of additional physical, chemical, and biological effects that control enzyme concentration/kinetics once an enzyme is released into the environment, such as enzyme lifetime/denaturation, diffusion (Vetter et al. 1998, Rothman and Forney 2007, Allison et al. 2011, Sinsabaugh and Follstad Shah 2012), sorption (Mayer 1994), water potential, temperature, pH, and competitive inhibition. As a result, measures of activation energy can vary greatly for the same enzyme in similar soil systems (Sinsabaugh and Follstad Shah 2012). Over 50 different enzymes are known to degrade cellulose alone in cow rumen (Hess et al. 2011); orders of magnitude more are likely responsible for decomposing the diversity of compounds found in soil and litter. Enzymatic diversity in these models (Allison 2012, Sinsabaugh and Follstad Shah 2012, Gangsheng et al. 2013) is far less. The death rates and/or dormancy of microbial populations is also heterogeneous and also not well understood. Despite the number of advances in our understanding of organic matter degradation systems during the past decade, many of the limiting mechanisms responsible for decomposition kinetics remain uncharacterized, and appropriate levels of abstraction have not yet been determined. These problems collectively suggest the need to estimate and model complex heterogeneous transformations in the absence of complete physical transport and biochemical information.

Here we test the limits of a simpler model of organic matter decomposition and find that it provides new insights for estimating and describing decomposition dynamics. This paper makes three principle contributions. First, we show that simple models of parallel heterogeneous organic matter decomposition (Boudreau and Ruddick 1991, Bolker et al. 1998, Manzoni et al. 2009, Forney and Rothman 2012*a*) can also describe a transformation continuum under certain assumptions. Decay rates from these models represent rates of carbon exit from a transformation network, rather than as isolated spontaneous exponential decays. Next, we provide a method for estimating the underlying kinetics of these decomposition networks and pathways from decay data. Finally, we use the kinetic patterns to interpret properties of network structure.

Approach

Previously (Forney and Rothman 2012*a*) we utilized a continuous model of decay heterogeneity to analyze decay data from the Long-term Inter-site Decomposition Experiment, (LIDET) (Harmon and Lidet 1995, Gholz et al. 2000, Harmon 2007, Adair et al. 2008, Cusack et al. 2009, 2010, Harmon et al. 2009). In that model, organic matter is assumed to decay with heterogeneous kinetics, described by a distribution of first-order decay rate constants k. The fraction $g(t)$ of organic mass remaining is a superposition of exponential decays:

$$g(t) = \int_0^\infty p(k)e^{-kt}dk \qquad (1)$$

where $p(k)$ is a probability distribution having the properties $p(k) > 0$ and $\int_0^\infty p(k)dk = 1$. By inverting Eq. 1 we found that $p(k)$ is on average lognormal. Therefore, organic matter decomposition from the LIDET study can be described by a two-parameter lognormal continuum of parallel decay rates.

Here we show that Eq. 1 can also describe decomposition proceeding through a complex network of transformation and decay mechanisms. In this manner, $p(k)$ represents the distribution of Poisson rates at which particles exit from all pathways in the network. By estimating $p(k)$ we capture the mass dynamics of the system without needing to model the details of transformations across the entire network. We show that, for the case of the LIDET study, the same lognormal decay rate distribution well approximates the rates of exit from a stochastic network of transformation processes. Interpreting the network as

$p(k)$ provides a unique way to visualize and pinpoint key dynamic information regarding carbon in the system and reveals the timescales of the retention of organic carbon in decomposition systems. Dynamic properties such as turnover time of organic carbon are very sensitive to the heterogeneity of timescales associated with underlying decay processes (Sierra et al. 2011, Forney and Rothman 2012*a*).

The work presented here relates to previous efforts to simplify degradation models by eigenvalue decomposition and diagonalization (Bolker et al. 1998). Bolker et al. (1998) diagonalized small decomposition models such as the CENTURY model, which assume organic matter transforms between only a few different states. They calculated system eigenvalues (diagonalized decay rates) and interpreted the meanings of positive and negative weights (or loadings) of the diagonalized exponential decays. The CENTURY model was simplified by reducing the number of parallel compartments and parameters needed to equivalently describe organic matter decay, and they suggested further simplifications may be obtained by assuming a distribution of parallel rates. Here, however, we consider transformations between states that take place heterogeneously at a distribution of rates. We build upon the previous work by using the diagonalized parallel approach to describe the heterogeneous organic matter transformation continuum and provide an inverse method for determining its shape.

To achieve this goal we need to assume that transformations are linear. This linearity assumption is consistent with the following situations: that the soil microbial community is essentially in a steady state upon litterfall, and that any growth in microbial populations on a particular substrate happens fast relative to the litter turnover time of ~10 years (Forney and Rothman 2012*a*). Because transformation timescales for different substrates can vary widely, we approximate them to an order of magnitude by a first-order reaction, and allow for many different rates of transformation for each substrate compound. These rates may depend on different types of enzymes, physical transport of enzyme and substrate, and the enzyme concentration governed by the various factors described above: enzyme lifetime, signal pathways, and cost of enzyme production (Vetter et al. 1998, Allison 2012), and steady-state sizes of populations governed by predation, competition, and/or other resources.

The remainder of our paper is organized as follows. In the next section we introduce decomposition in terms of network of heterogeneous reactions. We present a simple two-state network as a simple illustration of the methods used throughout the paper. In the following section we introduce the-exit-rate function and show how it describes a decay system with a continuum of transformations. We next explore examples of compartmental decomposition systems where mass exchange between compartments takes place at a distribution of rates. We investigate the properties of heterogeneous compartments in series and in feedback. This includes investigating the behavior of the CENTURY terrestrial respiration model (Parton et al. 1987) with compartments that have heterogeneous kinetics. Here we also consider the case of a more general stochastic system composed of a continuum of plant litter, microbial, and soil organic matter states. In the next section we calculate the distribution of rates associated with the LIDET data sets constrained so that these rates represent the exit rates from a transformation network. Finally, in the last section, we find that the distribution of exit rates from the network is approximately lognormal, and can be approximated by a parallel system.

Definitions of the symbols and variables we use throughout are presented in Table 1.

Degradation as a Network of Transformations

We describe decomposition as a network of reactions that transform organic carbon between a widely dispersed network of states. Transformations to and from each state occur at many rates depending on physical and chemical conditions, decomposer community, and other stochastic variables. In other words, transformations are related to both bioavailability—whether appropriate enzymes that can cleave the substrate are available (Semple et al. 2004)—and bioaccessibility—whether an appropriate decomposer can physically access the substrate (Semple et al. 2004). These transformations likely occur among a continuum of soil organic matter (SOM) states (Carpenter 1981, Bosatta 1985, Melillo et al. 1989, Ågren and Bosatta 1998, Sierra et al. 2011). With this in mind, we suggest that organic matter transforms between a distribution of states, at a distribution of rates.

We proceed by quantitatively tracking a carbon atom on its journey through various states in a decomposition network. For example, a carbon atom might enter the system as an organic plant polymer state (perhaps protected by lignin). It may then transform to an unprotected polymer state and eventually be released as a smaller polymer, dissolve, sorb to a clay, be cleaved to a monomer, become part of microbial structure, transform to another biological structure, released as an enzyme, and/or interact chemically with other environmental compounds. Eventually, a microbe may completely oxidize the organic carbon to CO_2. We assume that each state transformation is governed by a limiting environmental and/or ecological process operating in a steady state. We consider two equivalent ways of describing the movement and transformation of mass among different states. One method is to use a deterministic model, which describes the multi-state system by a set of first-order linear differential equations. The other method is to consider a stochastic model, where particles have a given probability of transforming

TABLE 1. Summary of symbols and variables used throughout together with their explanations/definitions.

Symbol	Definition
t	time
G	total system mass
G_0	initial system mass
g	fraction of initial mass remaining in the system; $g = G/G_0$
$\boldsymbol{x}$	vector of all state masses
$x_{i,j}$	mass of state j in pool i
n	number of states per pool
$k_{i,j}$	rate of transformation out of state j in pool i
$p_{i,j}$	mass fraction entering pool i partitioned into state j
$f_{i,j,l}$	conversion fraction (fraction of mass transferred from state j in pool i, to pool l)
$1 - \sum_j f_{i,j,l}$	fraction of mass going to the exit or absorbing state: inorganic carbon or leached carbon
$\mathbf{A}$	decay system matrix
y	total number of pools in the network
z	total number of states in the network
λ_i	ith eigenvalue of the decay matrix $\mathbf{A}$
$\mathbf{\Lambda}$	$z \times z$ eigenvalue matrix with diagonals λ_i
$\mathbf{u_i}$	ith eigenvector of the decay system $\mathbf{A}$
$\mathbf{U}$	$z \times z$ eigenvector matrix having columns $\mathbf{u}_i$
$\mathbf{S}$	$z \times z$ diagonal matrix with ith diagonal $1 = \sum_j u_{i,j}$
$\mathbf{r}$	vector containing the initial mass fractionation (weights) associated with the eigenvalues
r_i	initial mass fractionation onto the eigenvalues k of a decay system with a continuum of states (continuous distribution of exit rates k; exit-rate function)
$v(\ln k)$	continuum of exit rates in log rate space (log exit-rate function)

from one state to another over a small time period. The two approaches are equivalent for the purpose of describing overall mass dynamics of degradation systems. Both types of models have been used to model decomposition but often contain a small finite number of states. The stochastic approach has been implemented via both a Markov process (Sierra et al. 2011) and an absorbing Markov chain (Liang et al. 2010). The deterministic approach is more common, usually implemented via compartmental models such as CENTURY (Parton et al. 1987), Roth-C (Jenkinson et al. 1990), the carbon turnover model of Van Veen and Paul(van Veen and Paul 1981), and many others (Manzoni and Porporato 2009). These compartmental models are equivalent to continuous-time Markov processes. In all of these models, transformations between states occur continuously in time at the rates k. The main characteristic of Markov processes is transformations of particles from one state to another are memory-less (depend on only the current state). In this paper we often use the deterministic formulation to calculate dynamic properties of the system. However it is helpful to keep the stochastic Markov interpretation in mind when thinking of organic carbon transformations. We provide stochastic interpretations when relevant.

Two-state example

Fig. 1 shows a pedagogical device where organic matter exists in just two states: an initial state (fresh litter organic component) and a transformed state (chemically transformed structure, physically altered micro environment, etc). We assume transformations from the initial state occur at the first-order rate constant k_1, with probability f of transforming to the second state, and probability $(1 - f)$ of transforming

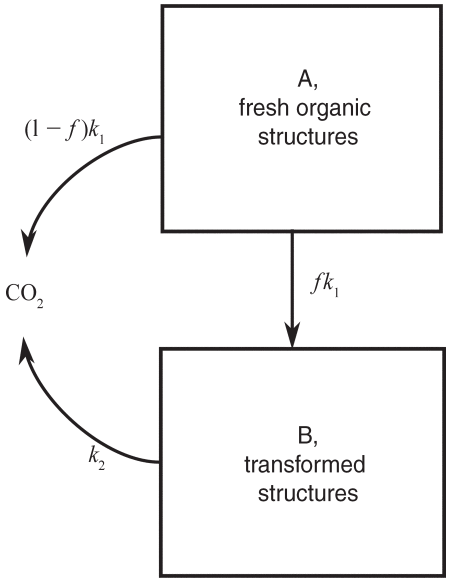

FIG. 1. A two-state network. State A may be interpreted as a fresh litter structure, and state B a transformed organic structure. Particles leave the first state at a first-order rate k_1. These particles transfer to the second state with a probability f and therefore transform at the rate $f k_1$. Particles transfer from the first state to the exit state, CO_2, at the rate $(1 - f)k_1$. In this simple model, particles transform from the second state only to the exit state and do so at the rate k_2.

to the exit state (carbon dioxide). Carbon in the second state then exits at the rate k_2. The dynamics of this simple system follow Eqs. 2 and 3, where x_i is the concentration or amount of carbon in state i:

$$\frac{dx_1}{dt} = -k_1 x_1 \tag{2}$$

$$\frac{dx_2}{dt} = -k_2 x_2 + fk_1 x_1. \tag{3}$$

Eqs. 2 and 3 can be more compactly written in matrix form as

$$\frac{\mathrm{d}\mathbf{x}}{\mathrm{d}t} = \mathbf{A}\mathbf{x} \tag{4}$$

where

$$\mathbf{x} = \begin{bmatrix} x_1 \\ x_2 \end{bmatrix}, \quad \mathbf{A} = \begin{bmatrix} -k_1 & 0 \\ fk_1 & -k_2 \end{bmatrix} \tag{5}$$

having the initial condition $\mathbf{x}(0)$.

The solution $\mathrm{x}(t)$ is derived in Appendix A and is a superposition of two exponential decays:

$$\mathbf{x} = \alpha_1 \mathbf{u_1} e^{-\lambda_1 t} + \alpha_2 \mathbf{u_2} e^{-\lambda_2 t} \tag{6}$$

where $\mathbf{u}_i$ are the eigenvectors of the system and α_i are the weights for each exponential decay.

Substituting the initial condition $\mathbf{x}(0)$ into Eq. 6 provides the weights α_i. The total mass of the system, $G(t) = x_1(t) + x_2(t)$ therefore decays as

$$G = r_1 e^{-\lambda_1 t} + r_2 e^{-\lambda_2 t} \tag{7}$$

where r_i is determined by summing the states x_i of Eq. 6:

$$\begin{bmatrix} r_1 \\ r_2 \end{bmatrix} = \begin{bmatrix} \sum_i u_{1,i} & 0 \\ 0 & \sum_i u_{2,i} \end{bmatrix} \begin{bmatrix} \alpha_1 \\ \alpha_2 \end{bmatrix}. \tag{8}$$

Here $u_{1,i}$ are the components i of the eigenvector $\mathbf{u_1}$ and $u_{2,i}$ are the components i of the eigenvector $\mathbf{u_2}$, $i = 1, 2$. For the system (Eqs. 5), the values of r_i are

$$r_1 = x_1(0)\left(1 + \frac{fk_1}{k_2 - k_1}\right) \tag{9}$$

$$r_2 = x_2(0) - x_1(0)\frac{fk_1}{k_2 - k_1}. \tag{10}$$

The lesson of this elementary exercise is that although the system contains two pools in series, its total mass decays as if it were two pools in parallel (Bolker et al. 1998, Manzoni et al. 2009). The weights r_i of each exponential decay are related to both the eigenvectors of the system and the initial conditions. Furthermore, the rates of parallel decay reflect the rates of the underlying serial pools. These properties are consistent with all examples of decomposition networks throughout the paper.

A continuum of transformations

We now suppose that pools of carbon are composed of heterogeneous particles and that transformations between pools occur over a distribution of rates. We introduce this concept by fractionating each compartment in the simple model of Fig. 1 into a distribution of n states. These particle-states (pseudo-compartments (Matis and Wehrly 1998)) transform at random rates (Matis et al. 1989) as shown in Fig. 2.

The heterogeneous transformations shown in Fig. 2 may be represented by the set of $2n$ first-order differential equations which includes all states:

$$\begin{aligned} \frac{dx_{1j}}{dt} &= -k_{1j}x_{1j} + J(t)p_{1j} \qquad j = 1, \ldots, n \\ \frac{dx_{2j}}{dt} &= -k_{2j}x_{2j} + p_{2j}\sum_{i=1}^{n} f_{1i}k_{1i}x_{1i} \qquad j = 1, \ldots, n. \end{aligned} \tag{11}$$

Here, x_{1j} is the mass associated with the jth state in carbon pool 1, and x_{2j} is the mass associated with the jth state in carbon pool 2. The probability p_{ij} partitions mass incoming to the ith pool into the state j and has values such that $\sum_j p_{ij} = 1$. If transformations are microbial, the conversion fraction f_{ij}, represents a substrate utilization (carbon uptake) efficiency (Manzoni and Porporato 2007, Feng 2009, Manzoni et al. 2010). It is the probability that carbon involved in the jth process will be transformed to a microbial component, while $(1 - f_{ij})$ is the probability that the carbon will be respired to CO_2. The conversion fraction f_{ij} can also be associated with more general losses from the system, such as the leaching of carbon to groundwater from certain states, or abiotic oxidation such as photo-oxidation or ozone-oxidation (Carr and Baird 2000). Allowing the transformation rates and conversion fractions to be random provides a more general and realistic description of complex heterogeneous decay networks.

We can write this dynamics of the linear system (Eqs. 11) in matrix form, just as we did in Eq. 4, as

$$\frac{d\mathbf{x}}{dt} = \mathbf{A}\mathbf{x} + J(t)\mathbf{p_0} \tag{12}$$

where $J(t)$ is the input of fresh dead organic matter to the system and $\mathbf{x}$ and $\mathbf{p_0}$ are the concatenated vectors:

$$\mathbf{x} = \begin{bmatrix} \mathbf{x_1} \\ \mathbf{x_2} \end{bmatrix} \qquad \mathbf{p_0} = \begin{bmatrix} \mathbf{p_1} \\ \mathbf{0} \end{bmatrix}$$

$$\mathbf{x_1} = \begin{bmatrix} x_{11} \\ \vdots \\ x_{1j} \\ \vdots \\ x_{1n} \end{bmatrix}, \quad \mathbf{x_2} = \begin{bmatrix} x_{21} \\ \vdots \\ x_{2j} \\ \vdots \\ x_{2n} \end{bmatrix}, \quad \mathbf{p_1} = \begin{bmatrix} p_{11} \\ \vdots \\ p_{1j} \\ \vdots \\ p_{1n} \end{bmatrix}. \tag{13}$$

The components of $\mathbf{x}_i$ of pool i are the states $x_{i,j}$ and the components of $\mathbf{p_1}$ are p_{1j}. The vector $\mathbf{p_0}$ represents the

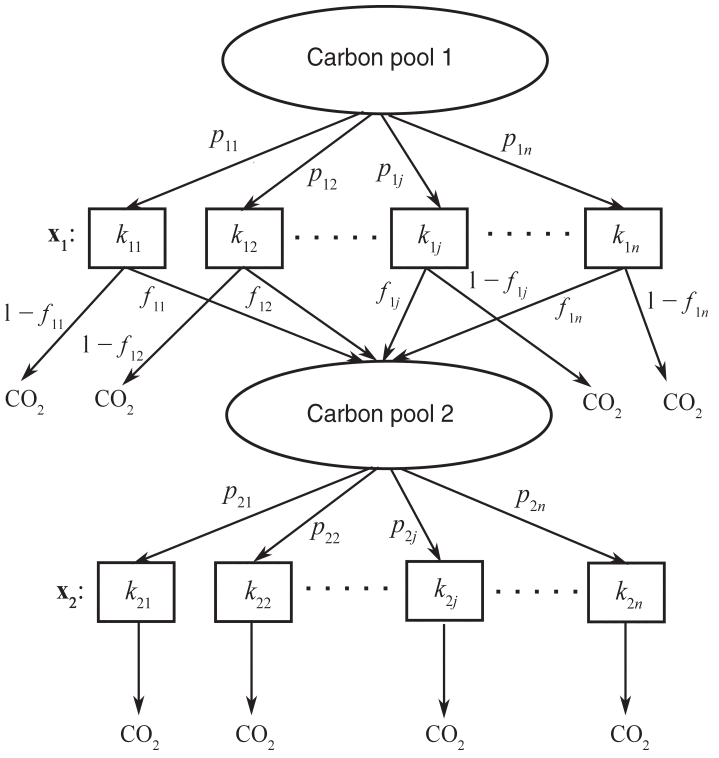

FIG. 2. Serial processes with distributed rates. Transfers between pools of organic matter occur over a distribution of rates. Ovals represent macroscopic pools of organic matter, while boxes represent the fractionation $\mathbf{p}$ of the preceding pool into different states x that transform at different rates k. Mass fractions f are transferred to the next pools, while the fractions $1 - f$ are mineralized or otherwise lost from the system. If the processes are biotic, carbon may be respired to CO_2, and only a fraction of carbon is passed to the next pool. Carbon in the first pool is partitioned into states $\mathbf{x_1}$ by the fractionation vector $\mathbf{p_1}$, with p_{1i} determining the fraction of mass going to state x_{1i}. Each state transforms at a random rate k_{1i} and passes to pool two with the probability f_{1i}. Mass incoming to pool 2 is partitioned into states $\mathbf{x_2}$ with mass fractions specified by $\mathbf{p_2}$. All states decay at the random rates k_{2i} to CO_2.

initial fractionation of incoming fresh dead organic matter into the network. The vectors $\mathbf{x}$ and $\mathbf{p_0}$ have length z, the total number of states in the system.

Eq. 12 describes more generally any network of y pools connected with distributed rates. In the more general case, $\mathbf{x} = [\mathbf{x_1}, \mathbf{x_2}, \ldots \mathbf{x_y}]^\top$ represents the states within all pools and $\mathbf{p_0}$ contains the partition vectors $\mathbf{p}_i$ of all pools which initially receive mass, rescaled so that $\sum_j \mathbf{p}_{0,j} = 1$.

The solution to this system when the input $J(t)$ is an initial impulse of size G_0 is

$$\mathbf{x} = G_0\ \mathbf{U}e^{-\mathbf{\Lambda}t}\ \mathbf{U}^{-1}\ \mathbf{p_0} \tag{14}$$

as derived in Appendix B. The matrix $\mathbf{U}$ contains the eigenvectors of $\mathbf{A}$, $\mathbf{u}_i$:

$$\mathbf{U} = [\mathbf{u_1}\ \mathbf{u_2}\ \cdots\ \mathbf{u}_z]\ . \tag{15}$$

$\mathbf{\Lambda}$ is a diagonal matrix containing the eigenvalues of $\mathbf{A}$:

$$\mathbf{\Lambda} = \begin{bmatrix} \boldsymbol{\lambda}_1 & 0 & \cdots & 0 \\ 0 & \boldsymbol{\lambda}_2 & \cdots & 0 \\ \vdots & \vdots & \ddots & \vdots \\ 0 & 0 & \cdots & \boldsymbol{\lambda}_z. \end{bmatrix} \tag{16}$$

and $e^{-\mathbf{\Lambda}t}$ is the matrix exponential. The total mass remaining in the decay system is

$$G(t) = \sum_i x_i(t). \tag{17}$$

Substituting the elements of $\mathbf{x}$ in Eq. 14 for x_i in Eq. 17 provides the dynamics of the total mass remaining in the system as a function of time:

$$g(t) = \sum_i r_i e^{-\lambda_i t} \tag{18}$$

where $g(t)$ is the mass fraction remaining in the system $G(t)/G_0$ The decay (Eq. 18) is now expressed as a sum of parallel exponential decays. The eigenvalues λ_i are the rates at which carbon exits the decay network. The weights r_i are the elements of the vector

$$\mathbf{r} = \mathbf{S}\mathbf{U}^{-1}\ \mathbf{p_0} \tag{19}$$

that partitions the incoming mass into the parallel decays. Because all states x_i are summed in order to calculate $g(t)$, the matrix $\mathbf{S}$ contains the sum of each eigenvector $\mathbf{u}_i$ (see Appendix B1)

$$\mathbf{S} = \begin{bmatrix} \sum_j u_{1,j} & 0 & \ldots & 0 \\ 0 & \sum_j u_{2,j} & \ldots & 0 \\ \vdots & \vdots & \ddots & \vdots \\ 0 & 0 & \ldots & \sum_j u_{z,j} \end{bmatrix}. \tag{20}$$

Since $\mathbf{r}$ derives from the projection of the initial state vector $\mathbf{p_0}$ onto the eigenvectors, there is no reason for the elements of the projected vector $\mathbf{r}$ to remain positive. We find that these negative components are related to a time lag rather than a decay. Furthermore, there is no constraint on the system $\mathbf{A}$ to have real eigenvalues.

However because eigenvectors come in complex conjugate pairs, values of r_i cannot be complex. Nevertheless, decomposition systems appear to be dissipative enough that complex eigenvalues are not prevalent; we return to complex eigenvalues in our discussion of feedback in *Example systems: Feedback processes*.

We now note that the stochastic Markov description of carbon dynamics aids the interpretation of carbon movement throughout the decomposition network. The probability P_{ij} that a particle in state i at time 0 will be in state j at time t is as follows (Matis and Wehrly 1998, Matis et al. 1983):

$$\mathbf{P}(t) = e^{\mathbf{A}t} = \mathbf{U}e^{\Lambda t}\ \mathbf{U}^{-1} \tag{21}$$

where $\mathbf{P}$ is the $z \times z$ matrix with elements P_{ij}, $\mathbf{A}$ is the same matrix in Eq. 12 that contains the transition or transformation rates k. $\mathbf{U}$ and Λ contain the eigenvectors and eigenvalues of $\mathbf{A}$. Similarly, the survival probability at time t of particles that were initially distributed among the states $\mathbf{p_0}$ at $t = 0$ is equivalent to the impulse response $g(t)$ given by Eq. 18 (Faddy 1990, Matis and Wehrly 1998). An additional insightful property is that the mean residence time of particles in state j that originated in state i is given by the elements of the matrix $\mathbf{A}^{-1}$ (Matis et al. 1983, Matis and Wehrly 1998).

Obtaining the Exit-rate Function $r(k)$ from a Network

Transformations between pools are more likely to occur at a continuous distribution rather than a discrete distribution of rates. Therefore it is natural to expect there to be a continuum of exit rates k from the system. The mass remaining in the system is then described by the continuous superposition:

$$g(t) = \int_0^\infty r(k)e^{-kt}dk \tag{22}$$

which is the continuous version of Eq. 18. The exit-rate function $r(k)$ provides the weights associated with the rates that carbon exits the continuous-transformation system. Details of the extrapolation of the discrete network model to the continuum can be found in Appendix C.

Eq. 22 shows that the mass lost from a decay system can be interpreted as the Laplace transform of the exit-rate function $r(k)$. It indicates that the parallel description of organic matter decay is simply a projection of the complete system onto the coordinates $\mathbf{U}$. In this manner, the impulse response is described in terms of the eigenvalues of the underlying decay system. Eq. 22 is equivalent to the original parallel decay Eq. 1 except that $r(k)$, like $\mathbf{r}$, may be negative. Ultimately, we seek to invert decay data in order to find the exit-rate distribution $r(k)$ for a litter-decay data set. But first, we calculate and interpret $r(k)$ for various examples of network configurations.

Example Systems

In this section we calculate and interpret the exit-rate function $r(k)$ for four examples of network configurations: (1) serial networks, (2) feedback networks, (3) the CENTURY degradation model which contains parallel, serial, and feedback processes, and (4) an amorphous network containing a continuum of interconnected states. These examples help to develop an intuition for interpreting $r(k)$.

Calculating r(k) from a network with heterogeneous states and distributed rates

In each of these cases, we prescribe a network configuration and calculate the exit-rate distribution $r(k)$ associated with it. To numerically determine $r(k)$ associated with a given network, we use a Monte Carlo simulation with N trials in order to estimate a mean $r(k)$. This is discussed in detail in Appendix D. Because we assume rate heterogeneity is wide, we change variables from $k \rightarrow \ln k$ and calculate $v(\ln k)$, which is equivalent to $r(k)$ in $\ln k$ space.

$v(\ln k)$ and $r(k)$ are related by the equation $v(\ln k) = r(k)[d \ln k^{-1}/dk]$. The mass fraction remaining expressed in terms of $v(\ln k)$ is

$$g(t) = \int_{-\infty}^{\infty} v(\ln k)e^{-kt}d\ln k. \tag{23}$$

Serial pools

Here we calculate and interpret $r(k)$ resulting from multiple pools connected in series. We first consider two pools in series as shown in Fig. 2. The mass entering each pool is partitioned into different rates by the distributions $p_1(k)$ and $p_2(k)$. In this and the remaining examples we choose the distributions to be lognormal. We assume this based on the finding that decay rates are lognormally distributed (Forney and Rothman 2012*a*) and the related suggestion that organic matter quality may be lognormally distributed (Bosatta and Ågren 1991). We then use a Monte Carlo simulation to randomly sample 32 rates from each distribution, assemble the connectivity matrix $\mathbf{A}$, and then calculate its eigenvalue decomposition and associated $\mathbf{r}$. We repeat this process ~10 000 times to generate an ensemble of initial eigen-decay state vectors $\mathbf{r}$. We follow the procedure outlined in Appendix D to estimate the ensemble average $v(\ln k)$. Fig. 3A reveals that the average $v(\ln k)$ is smooth, has one inflection point, and becomes negative in the faster portion of the spectrum. The positive region of $v(\ln k)$ resembles the lognormal distribution associated with the slower transformations in the serial network.

When a network consists of pools in series, the full system matrix $\mathbf{A}$ can be written as a lower triangular matrix, because information only flows in one direction. A relevant property of the triangular matrix $\mathbf{A}$ is that its

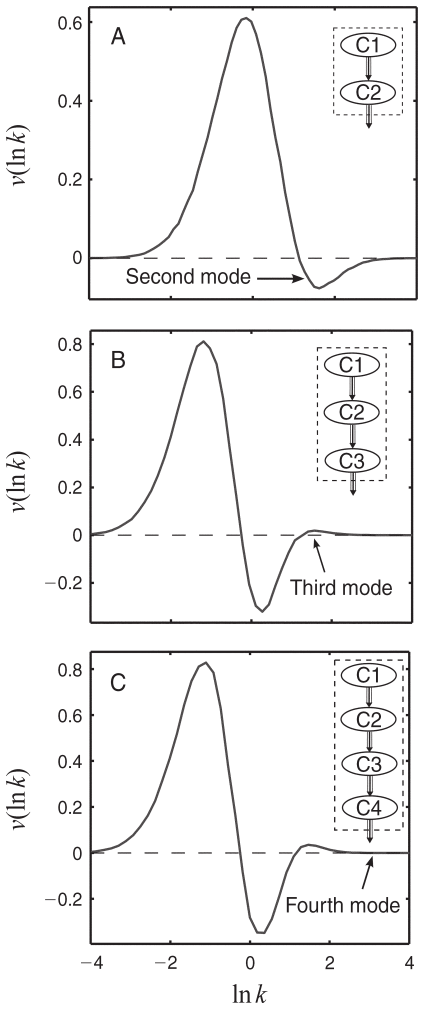

FIG. 3. Exit-rate functions $v(\ln k)$ associated with distributed serial processes. To generate each plot, each pool is fractionated among 32 states that decay at rates randomly chosen from a distribution $p_i(k)$ associated with the ith pool. We estimate the exit-rate function $v(\ln k)$ using the Monte-Carlo procedure given in *Obtaining the exit-rate function r(k)*.... All mass is allocated in the first pool at $t = 0$ and mass only exits the system from the final pool in the series; $f = 1$ for all transformations. (A) $v(\ln k)$ corresponding to two pools in series. Carbon leaves the first pool at a distribution of rates $p_1(k)$ and leaves the second pool according to the distribution $p_2(k)$. $p_1(k)$ is lognormal with a mean and variance of log k equal to 0 and 1, respectively. $p_2(k)$ is lognormal with a mean and variance of log k equal to -1 and 1, respectively. We used 8000 realizations of the discrete exit-rate vector **r** to approximate the continuous function $v(\ln k)$. (B) Three pools in series. Flows out of each pool are set by the distributions $p_1(k)$, $p_2(k)$, and $p_3(k)$. The mean and variance of log k for each distribution is as follows: p_1, 0 and 1; p_2, -1 and 1; p_3, 1 and 1; 10 000 trials. (C) Four pools in series. Flows out of each pool are given by the same distributions p_1, p_2, p_3 in (B). The flow out of the fourth pool is set by p_4, which is lognormal with a mean and variance of log k equal to 3 and 1; 10 000 trials.

diagonals, which represent the rates of state transformations, are also its eigenvalues. Therefore the exit rates are closely related to the underlying transformation rates in the system.

Because mass must pass through both a slow and fast pool before exiting, a negative mode appears in $r(k)$ around the rates of the fast pool. This occurs because the system eigenvalues are still the diagonals of **A**, but matter cannot exit the system at the rapid rates of the fast pool. To compensate, the weights $r(k)$ take on negative values at these faster rates, indicating a lag or delay at those time scales.

We repeat this process for systems containing three and four lognormal pools in series with varying mean and variance of In k. The exit-rate functions for these systems are presented in Fig. 3B and C. We find that the number of modes can reflect the number of kinetically distinct compartments in the network. The sign of the modes however is related to the mass loss, or conversion fraction f, associated with transfers from that pool. If enough mass exits the system from a pool, the function $v(\ln k)$ may remain positive over the rates $\ln k$ associated with that pool. If little mass is lost and more mass is transferred at rates $\ln k$, negative modes may be associated with those rates. The negative mode signifies a lag time associated with those processes. Because rate distributions of pools may overlap, the number of modes in the distribution $r(k)$ indicates a lower bound on the number of macroscopic processes in series. The exact number of serial processes can be estimated from $r(k)$ and $g(t)$ by using the "phase function method" (Zhou and Zhuang 2006) when decay data have high resolution near $t = 0$ (Zhou and Zhuang 2007).

This approach fails however, as do the standard popular compartmental terrestrial decomposition models, when there is a long lag time, or inoculation time, before the onset of decomposition. A long lag time may result from highly serial processes or when no transformations occur, such as when an organic substrate is being inoculated. Purely serial processes with random rates result in a system with a generalized Erlang distribution of residence times (Faddy 1990, Neuts 1995). Because of the large lag or delay time associated with long chains of purely serial processes, Monte Carlo simulations show large rapid fluctuations in the weights of the projected eigen-decay states **r** and fail to generate a stable mean $r(k)$. However, if a large lag time actually represents an inoculation time where no transformations occur, modeling this waiting time via many serial transformation processes is likely inappropriate. Rather, we suggest modeling the inoculation time with a simple lag time parameter, a, by transforming time to $t^* = t - a$.

Feedback processes

Feedback loops are fundamental to decomposition systems since decomposers recycle old organic matter into new biomass that remains part of the soil organic matter decomposition system. We suggest that feedback between carbon pools takes place stochastically at different rates, as shown in Fig. 4A. In this section we consider simple arrangements of pools in feedback to generate the system matrix **A** and calculate its eigenvalue

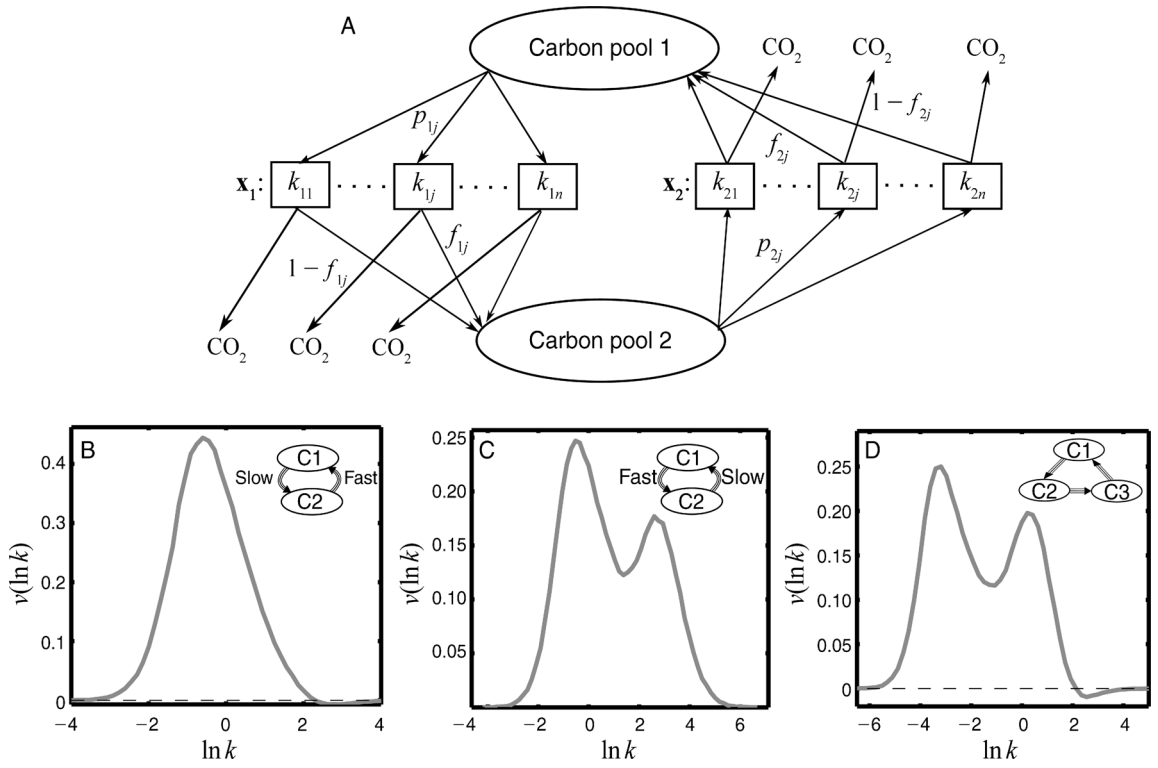

FIG. 4. Feedback processes with distributed rates. (A) Feedback between two pools with distributed rates. (B) Exit-rate function of two carbon pools in feedback. Pool C1 decays with 32 random rates sampled from a distribution p_1 and pool C2 decays with 32 random rates sampled from a distribution p_2. p_1 and p_2 are both lognormal with a mean and variance of log rates as follows: p_1, 0, 1; p_2, 2.5, 1. All states have the same conversion fraction $f = 0.5$. Only a few eigenvalues are complex, indicating oscillations in some eigenstates. However in those cases, imaginary components were less than 5% of the decay rates. This figure uses an ensemble of 8000 randomly generated trials of **r**. (C) Exit-rate function of two pools in feedback, with rate distributions p_1 and p_2 opposite of (A). The mean and variance of log rates of these distributions are p_1, 2.5, 1, and p_2, 0, 1. All states have $f = 0.5$. Changing the order of C1 and C2 strongly influences $v(\log k)$. There are 4000 trials. (D) Exit-rate function of three carbon pools in feedback. The three distributions p_1, p_2, and p_3 are lognormal with a mean and variance of log k as follows: p_1, 0,1 ; p_2, 2.5, 1; p_3, −2.5, 1. All states have $f = 0.7$; 4000 trials.

decomposition, using the same procedure outlined in *Obtaining the exit-rate function...*, to identify the exit rates associated with feedback decay.

The exit-rate functions of three different feedback loops are shown in Fig. 4B–D. We first consider two pools in series connected by two lognormal distributions of rates p_1 and p_2, with a conversion fraction $f = 0.5$ associated with each transformation. The rates drawn from p_1 are two natural orders of magnitude (a factor of e^2) slower than the rates drawn from p_2. In the first case, Fig. 4B, incoming mass first enters the slowly decaying pool and then feeds into the faster pool. The exit-rate function $v(\ln k)$ is shifted slightly left of p_1(which has a mean ln k of 0) since particles may cycle through the system more than once before exit. In Fig. 4C the pools are switched with the fast pool decaying first followed by the slow pool. Because 50% of the mass exits after the fast pool, the signal from the fast pool becomes strong, appearing as a second mode in the exit-rate function. The order of transformations may therefore influence the eigenstate distribution $r(k)$. Fig. 4D shows the exit rates associated with three pools in series, with 70% of mass retained at each transformation (30% lost to CO_2). The medium and slow modes dominate, while the fast mode highlights the serial nature of the system.

Systems with feedback have a full **A** matrix and eigenvalues that may be complex (Bolker et al. 1998). Decays with complex eigenvalues take the shape of an exponentially damped oscillation. Real components of the eigenvalues represent exponential decay rates, while the imaginary components represent the frequencies of sinusoidal oscillations. However, in the test models of Fig. 4, the system matrices **A** are diagonally dominant. Most eigenvalues approximate the diagonals of **A** and <1% are actually complex. Furthermore, those which are complex typically have an imaginary component, $\Im(\lambda)$, less than 10% of the real component $\Re(\lambda)$, indicating a damping ratio (Greenberg 1998):

$$\zeta = \frac{1}{\sqrt{\left(\frac{\Im(\lambda)}{\Re(\lambda)}\right)^2 + 1}} \approx 1.$$

These decays are approximately critically damped (Greenberg 1998) and exhibit essentially no oscillation. Including the oscillatory components in the solution only changes the mass loss by a negligible amount and therefore only the real components of the eigenvalues are plotted on the horizontal axis of Fig. 4B–D. A multivariate $r(k)$ in complex rate space could be plotted; however the imaginary components do not reveal any further information about the decay in such systems and only complicate the picture.

Real soil carbon systems are also highly dissipative (Manzoni and Porporato 2007) as the conversion fraction, or substrate utilization (carbon uptake) efficiency, is small to moderate such that $0.1 < f < 0.7$ (Manzoni and Porporato 2007, Manzoni et al. 2008, 2010, Feng 2009), indicating that significant mass losses are associated with transformations. This property is reflected in calibrated models of decomposition networks (van Veen and Paul 1981, Jenkinson et al. 1990, Parton et al. 1993). As a result, both the Roth C and CENTURY models exhibit real eigenvalues for a wide range of system parameters (Bolker et al. 1998). We now proceed to investigate the CENTURY model with heterogeneous compartments.

Assembling compartmental models with distributed rates

Larger compartmental models with heterogeneous kinetics can be created by connecting pools to each other in parallel, series, and feedback with a distribution of rates. Contemporary compartmental models of soil organic matter decomposition (van Veen and Paul 1981, Parton et al. 1987, Jenkinson et al. 1990) typically connect pools with a single rate constant and do not account for a continuum of transformations.

By fractionating each compartment into a distribution of particle-states, the residence time of carbon in the pool is no longer exponentially distributed (Matis et al. 1989, Matis and Wehrly 1990). In fact, a compartment with any residence-time distribution can be approximated by fractionating that compartment into an appropriate arrangement of sub-states in series, parallel and/or feedback (Faddy 1990, Matis and Wehrly 1998). The residence time distribution associated with the passage through a network of linear compartments, Markov process, etc. is called "a distribution of phase type" (Faddy 1990, Neuts 1995, Matis and Wehrly 1998). Compartmental models containing pools with arbitrary residence-time distributions are called "semi-Markov models" (Matis and Wehrly 1990, 1998) and have been applied in fields such as pharmacokinetics (Matis et al. 1989, Matis and Wehrly 1990, 1998, Faddy 1990, 1993) to characterize heterogeneous absorption timescales and predict the concentration of a drug remaining in the body. We have assumed in this section that each compartment contains particle-states that are in parallel. The inversion method presented in *Analyzing LIDET data* allows for more general particle-state configurations.

Exit rates from the CENTURY model

Here we investigate the exit-rate function of the CENTURY model (Parton et al. 1987), assuming each compartment transfers carbon with a distribution of rates. In this modification of CENTURY, transfers occur among five carbon pools. Likely ranges of turnover times suggested for each pool are (Parton et al. 1987): (1) structural litter, 1–5 yr; (2) metabolic litter, 0.1–1 yr; (3) active soil, 1–5 yr; (4) slow soil, 20–40 yr; and (5) passive soil, 200–1500 yr. Their inverse provides a suggested range of turnover rates. Although pools likely have dispersed kinetics, the CENTURY model is highly parameterized in order to specify exact single rates of transfer between pools as a function of soil, litter type, and environmental conditions. Previously, an eigenvalue decomposition of the CENTURY model has revealed the model to behave as a parallel system (Bolker et al. 1998) for most conditions, seldom having negative values of $\mathbf{r}$ and complex rates λ.

Fig. 5 shows exit-rate functions from the CENTURY model (Parton et al. 1987) assuming pools have heterogeneous kinetics. The exit-rate function associated with case 1 is calculated by randomly assigning lognormal rates to 32 sub-compartments in each pool, assuming that the range of suggested turnover rates (Parton et al. 1987) represents four standard deviations of $\log k$. The mean of $\log k$ for each pool is assumed at the center of the suggested ranges. We use a Monte Carlo simulation as described in Appendix D to calculate the exit-rate function $r(k)$ from $N = 5000$ trials. The exit-rate function $v(\ln k)$ given these assumptions is shown as the green line in Fig. 5B. Each mode corresponds to a pool in the CENTURY model shown in Fig. 5B. This version of CENTURY has five pools, but only four modes are present in $v(\ln k)$ because pools 1 and 3 have the same suggested turnover times and therefore have similar eigenvalues. We then increase the variance of rates within the compartments and recalculate the exit distribution to show what happens as heterogeneity increases within each pool. The resulting exit-rate distributions associated with three changes in the variance are shown in Fig. 5. As the variance within each compartment increases, the properties of specific individual transformations in the network become less important, and for wide heterogeneity only a smooth continuum of rates prevails. Adding kinetic heterogeneity information counterintuitively reduces model parameterization, as the smooth exit-rate functions can be likely be described with fewer parameters than the base pools in CENTURY.

Considering that soil organic matter is a continuum, we suggest that proper parametrization of the exit-rate function in terms of decomposition controls such as

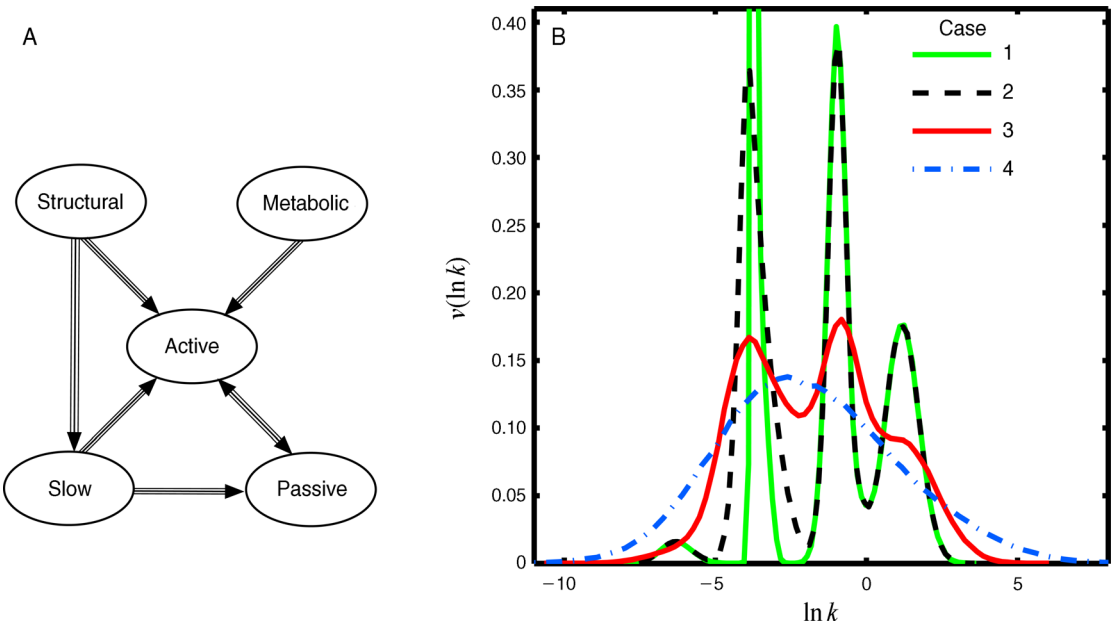

FIG. 5. Exit-rate function from the CENTURY model (Parton et al. 1987) assuming that pools have heterogeneous kinetics. (A) Architecture of the CENTURY Model. The model contains five pools: 1, structural; 2, metabolic; 3, active; 4, slow; 5, passive. (B) The log of the exit-rate function $v(\ln k)$ associated with four different choices of the rate variances σ_i; $v(\ln k)$ is calculated using the Monte Carlo method described in Appendix D. For each case, each pool has rates that are lognormally distributed. The mean log rate of each pool (μ_i) is set to the mean of the log of the turnover rates suggested in the text. For all cases, $\mu_1 = -0.80$, $\mu_2 = 1.15$, $\mu_3 = 0.80$, $\mu_4 = -3.34$, $\mu_5 = -6.31$. The variance of each pool σ_i^2 is set as follows. Case 1, solid green line: σ_i is set equal to the range of log rates for each pool divided by 4: $\sigma_1 = 0.40$, $\sigma_2 = 0.58$, $\sigma_3 = 0.40$, $\sigma_4 = 0.17$, $\sigma_5 = 0.50$. The range of suggested rates therefore span four standard deviations. Case 2, dashed black line: σ_i are the same as case 1 except σ_4 is increased to $\sigma_4 = 0.52$, roughly the same size as the other pools. Case 3, solid red line: all σ_i are increased by a factor of 2, $\sigma_1 = 0.80$, $\sigma_2 = 1.15$, $\sigma_3 = 0.80$, $\sigma_4 = 1.04$, $\sigma_5 = 1.00$. Case 4, dot dashed blue line: σ_i are further increased: $\sigma_1 = 1.61$, $\sigma_2 = 2.30$, $\sigma_3 = 1.60$, $\sigma_4 = 2.08$, $\sigma_5 = 2.01$. The range of suggested rates spans one standard deviation. For all cases, we assume plant matter to be surface litter with a lignin fraction of 0.16 and nitrogen fraction of 0.008. We also set the soil to have a combined silt and clay content of 0.75. These values determine the parameters associated with the fractionations between the pools in the CENTURY model (Parton et al. 1987).

substrate quality, climate, soil properties, may lead to more robust and accurate predictions of organic matter decay and turnover times. Prior results (Forney and Rothman 2012*a*) suggest that all rates in the decay rates scale similarly with changes in temperature and moisture. Because decomposition networks are dissipative, transformation rates in the network should also scale by the same amount with environmental change. This is consistent with the dependence of rates on temperature and moisture in the CENTURY model (Parton et al. 1993, 1987). The sensitivity of climatic parameters to transformation rates is discussed further in *Comparing the exit-rate function...*, below. A straightforward method to approximate the control of litter composition on the CENTURY exit-rate function is to apply the CENTURY-based effects of lignin and cellulose on rates to the median rates of each pool. With additional experimental verification, the relationships between pool variance and nitrogen and lignin content (Forney and Rothman 2012*a*) may also be applied. The exit-rate function can then be calculated from pools with composition-dependent parameters.

Amorphous networks

In this section we remove the concept of pools and consider soil as a mixed continuum of plant matter, microbial, and other transformed soil organic matter states. This is depicted in Fig. 6A. Initial litter states may transform to microbial or soil organic matter states at rates given by the distribution ρ_1, microbial states transfer to other microbial and soil organic matter states at rates given by ρ_m, and soil organic matter states transfer to other soil organic matter states and microbial states at rates given by ρ_s.

We calculate the exit-rate function $v(\log k)$ for a network composed of a number of litter, microbial, and soil organic matter states. Processes leading to a microbial state have a conversion fraction $f = 0.4$, consistent with estimates of substrate utilization (carbon uptake) efficiency (Manzoni and Porporato 2007, Manzoni et al. 2008, 2010, Feng 2009). The rates associated with litter, microbial, and soil organic matter states are randomly pulled from the lognormal distributions ρ_1, ρ_m, and ρ_s with parameters specified in the caption of Fig. 6B. States are also connected randomly for each trial to generate the system matrix **A**. As

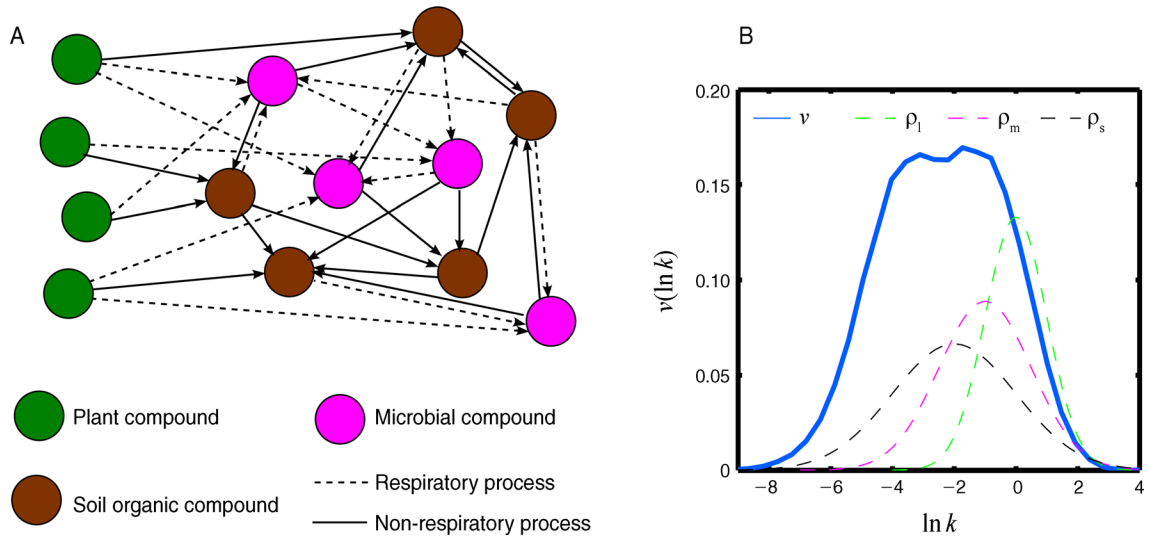

FIG. 6. (A) Transformation network between randomly configured litter, microbial, and soil organic matter states. Matter is initially allocated in litter states and is transformed to either microbial or other soil organic matter states. Transformation of carbon compounds to microbial states requires energy, and a fraction of carbon is converted to microbial structures via biosynthesis pathways ($f < 1$) while the remaining carbon is oxidized to carbon dioxide or other inorganic products via respiration pathways. While transformations between soil organic matter states may be microbially mediated, this carbon is not processed internally by the microbial cell and therefore does not take part in respiration ($f = 1$). (B) Exit-rate function $v(\ln k)$ for $N = 10\,000$ randomly configured networks consisting of 32 litter states, 32 microbial states, and 32 soil organic matter states (solid blue line). Mass flows initially from litter to microbial and soil organic matter states. Any flow to a microbial state has a conversion fraction $f = 0.4$. Litter states are randomly assigned from a lognormal distribution ρ_l (green dashed line) having a mean and standard deviation of log rates of 0 and 1, respectively. Microbial states are randomly assigned from a random distribution ρ_m (magenta dashed line) having a mean and standard deviation of log rates of −1 and 1.5, respectively, and soil organic matter states are assigned from a random lognormal distribution ρ_s (black dashed line) having a mean and standard deviation of log rates of −2 and 2, respectively. The distributions ρ_l, ρ_m, and ρ_s have been rescaled in the y direction for clarity.

described in Appendix D, we perform an eigenvalue decomposition to find the exit-rate vector **r** for $N = 10\,000$ random configurations of rates and connections in the network. We plot the rescaled sum of all exit rates $v(\log k)$ in Fig. 6B. Again we find that the **A** matrix is diagonally dominant, leading to eigenvalues that are approximately the same as the rates of the state transformations themselves. For this particular choice of parameters, $v(\log k)$ is roughly unimodal.

Analyzing LIDET Data

The previous sections discussed how the exit-rate function $r(k)$ relates to an underlying heterogeneous linear decay network **A**. The function $r(k)$ contains all of the information regarding mass loss from such a network. Because actual degradation networks are complex, modeling them well enough to forward-calculate a complete picture of $r(k)$ is nearly impossible. With only limited knowledge of the mechanisms and network structure, attempts at characterizing these networks require a large amount of empirical studies, approximations, heuristics, intuition, and curve fitting (Parton et al. 1987, 1993). Instead we suggest simply identifying $r(k)$ directly. We obtain $r(k)$ by inverting mass loss data from the LIDET data set (Harmon 2007). The inversion is constrained so that $r(k)$ represents a network of distributed serial, parallel, and/or feedback processes. To do so, we proceed with the log-transformed version of the exit-rate function $v(\ln k)$ and Eq. 23. Because Eqs. 22 and 23 are a Laplace transform, the function $v(\ln k)$ is obtained by calculating the inverse Laplace transform of $g(t)$. However, the inverse Laplace transform is ill posed (Hansen 1987, 1994, Lamanna 2005), meaning solutions $v(\ln k)$ are highly sensitive to data noise (Forney and Rothman 2012*b*). Regularization methods (Hansen 1987, 1994, Lamanna 2005) are commonly used to calculate the inverse Laplace transform of noisy data by seeking solutions with minimal degrees of freedom. Here we use Tikhonov regularization (Hansen 1987, Press et al. 1992) to identify an optimally smooth solution that best fits the data. We have previously applied this technique to Eq. 1 in order to identify the rate probability distributions $p(k)$ associated with litter-decay data sets (Forney and Rothman 2012*a*, *b*). Here $r(k)$ is not required to be a probability distribution, but its shape is nevertheless physically constrained. The physical constraints on the decay system are that the system mass cannot be negative:

$$g(t) \geq 0 \tag{24}$$

and the mass cannot increase,

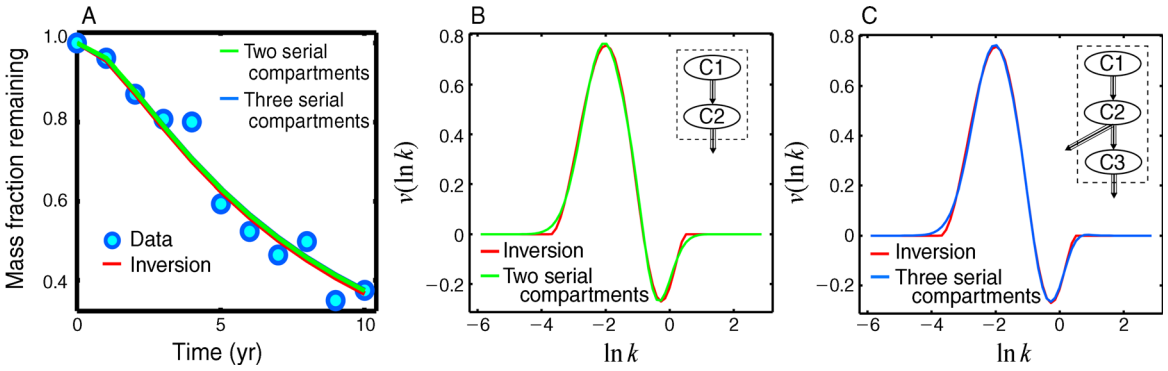

FIG. 7. Decay data and exit-rate function $v(\ln k)$ of a LIDET data set. (A) LIDET mass loss data (circles), mass loss prediction from the inversion (red line), two serial compartments (green), and three serial compartments (blue). (B) The red line is the exit-rate function calculated from the LIDET data set in panel (A). The green line is the exit-rate function corresponding to the best-fitting two-compartment serial network with lognormally distributed transformation rates. (C) The red line is the same as in panel (A). The blue line is the exit-rate function from the best-fitting three-compartment serial network with lognormally distributed transformation rates.

$$dg(t)/dt \leq 0. \tag{25}$$

To efficiently implement these constraints, we use the following approximations:

$$g(t) > 0 : \int_{-\infty}^{K} v(\ln k) d\ln k > 0 \tag{26}$$

$$dg(t)/dt < 0 : \int_{-\infty}^{K} -kv(\ln k) d\ln k < 0. \tag{27}$$

When $v(\ln k)$ is wide, e^{-kt} in Eq. 23 approximates a low-pass filter on $v(\ln k)$ at the rate $K = 1/t$; setting the integration limit to $K = 1/t$ approximates $v(\ln k)e^{-kt}$ well when $v(\ln k)$ is wide. When $v(\ln k)$ is not very wide, the constraints (26) and (27) are conservative approximations to (24) and (25). A proof is provided in Appendix E. With these approximations in mind, we evaluate the integral (27) at many limits K_i within the bounds of the function $v(\ln k)$ (see Appendix E) to ensure mass does not increase at any time t. Although the constraints (24) and (25) could be exactly evaluated, we implement constraints (26) and (27) for computational expedience.

Inversion of a LIDET data set

A decay time series from a LIDET data set is shown in Fig. 7A. The inversion $v(\ln k)$ of the data is shown as the red line in Fig. 7B. The inversion has one inflection point and becomes negative at fast k. In the negative region, mass is not exiting the system at those rates; rather the system exhibits lag or serial transfer at those rates because more mass is sequentially transforming at those rates than is exiting the system.

The exit-rate function $v(\ln k)$ in Fig. 7B may derive from a dissipative network comprised of a continuum of states that transform and decay at a continuum of rates. It may also similarly derive from a network of heterogeneous compartments. We test the hypothesis that this exit-rate function results from two or three heterogeneous pools in series. We first consider a two-pool serial network with lognormally distributed rates. The rates of transformation from pool 1 to pool 2 are described by the lognormal parameters μ_1 and σ_1. Mass leaves the system from pool 2 at lognormally distributed rates parameterized by μ_2 and σ_2. We assume mass transfers between pool 1 and pool 2 with a single conversion fraction f, although a distribution of conversion fractions f_{1j2} associated with each state could also be assumed.

We then use MATLAB's "nlinfit.m" function to fit the parameters μ_1, μ_2, σ_1, σ_2, and f to the to the exit-rate function $v(\ln k)$ that was inverted from the decay data. To do so, for a given value of μ_i, σ_i we discretize the pools over the domain of the inversion. We then use the eigenvalue decomposition of the discrete system to calculate the exit-rate function associated with those values of μ_1, μ_2, σ_1, σ_2, and f and compare it to the inversion. We find the parameters $\mu_1 = -0.18$, $\sigma_1 = 0.42$, $\mu_2 = -2.11$, $\sigma_2 = 0.63$, $f = 1.0$ best fit the $v(\ln k)$ from the inversion. The exit-rate function corresponding to these parameters is plotted as the green line in Fig. 7B. The conversion fraction $f = 1$ physically suggests the first compartment represents some distribution of inoculation rates, since all mass transfers to a second decomposition state without loss. Decay then proceeds heterogeneously in the second compartment. Because this transformation is loss-less, the pools may be reversed; the inoculation processes may be slow, whereas the inoculated decomposing state may decay fast. Since these compartments have heterogeneous kinetics, each compartment itself may represent a complex sub-network of reactions, transformations, and or other processes (Matis and Wehrly 1998).

We then consider a three-pool serial model with lognormal transformations. Mass exits the first pool at lognormal rates with parameters μ_1 and σ_1 and may transform to the second pool with conversion fraction f_{12} or to the third pool with conversion fraction f_{13}.

Mass exits the second pool at lognormal rates with parameters μ_2 and σ_2 and transforms to the third pool with conversion fraction f_{23}. (Again, we assume here for simplicity that the conversion fractions f_{ijl} of all states x_j associated with transfers from pool i to pool l are constant and use the shorter notation f_{il}.) Mass exits the third pool at lognormal rates with parameters μ_3 and σ_3. The parameters that best fit the inversion $v(\ln k)$ are $\mu_1 = -0.12$, $\sigma_1 = 0.50$, $\mu_2 = -2.11$, $\sigma_2 = 0.64$, $\mu_3 = 0.56$, $\sigma_3 = 0.40$, $f_{12} = 0.99$, $f_{13} = 0$, $f_{23} = 0.20$. Pools 1 and 2 from the three-pool network have similar properties as pools 1 and 2 from the two-pool network and represent a distributed inoculation time pool followed by a heterogeneous decomposition pool. No mass is transferred from pool 1 to pool 3. However, the parameter-fitting procedure identifies that 20% of the mass exiting the second pool enters a third pool having turnover times distributed between ~90 and 450 days. These turnover times are consistent with measured estimates of soil microbial turnover having substrate utilization efficiency of about 0.2 (Cheng 2009). We therefore suggest this pool is microbial. The exit-rate function calculated from the three pool network is the blue line in Fig. 7C. It provides a marginally better fit to the inversion than the two pool network of Fig. 7B. Even more realistic values may be encountered if we allow for feedback between pool 2 and 3. Decay prediction from the inversion and best fitting two- and three-compartment models are indistinguishable and plotted as the solid lines in Fig. 7A. The best-fitting distributions of transformation rates between the pools could be calculated using an additional inversion technique. However, this approach may be excessive as (1) the true underlying network architecture remains unclear and (2) the exit-rate function $v(\ln k)$ itself contains all information regarding mass loss from the network. Nevertheless, understanding the distributions of the underlying transformations might provide additional clues to how environmental and compositional drivers affect the overall exit-rate function $v(\ln k)$.

Inversion of 232 LIDET data sets

We proceed to calculate the regularized inverse for 232 LIDET data sets. We consider only the 237 LIDET data sets that contain five data points with replicates. Of those 237 we find five have insignificant mass loss after the first data point and we do not attempt to describe those data sets (Forney and Rothman 2012*a*). We find that the 232 inversions are either unimodal, bimodal, trimodal, or quadrimodal. Examples of each are shown in Fig. 8. We find that 38 are unimodal, 170 are bimodal, 12 are trimodal, and 7 are quadrimodal. Of the 38 unimodal solutions, 14 contain just one rate and decay exponentially. These are determined by calculating the nonnegatively constrained, unregularized inverse of the data (Forney and Rothman 2012*a, b*) and then checking whether that inverse contains just one rate and fits the data better than the regularized estimate of $v(\ln k)$.

The 12 trimodal $v(\ln k)$ can all be approximated by a simpler solution. Because the third mode of these data sets is a positive mode located at extremely fast rates, the entire mode decays to a negligibly small fraction by the time of the first measurement. In fact, for all of these solutions, the mass associated with this mode has decreased to approximately the double precision limit by the first data point and is effectively zero (Forney and Rothman 2012*b*). Therefore, this mass is experimentally equivalent to an instantaneous loss or leaching of mass. We thus suggest that the mass of the third mode is most simply represented by an instantaneous leaching of mass at $t \approx 0$ (Forney and Rothman 2012*b*). The inversion and its approximation (with the mass located at an infinite rate constant) is shown in Fig. 9A. Fig. 9C shows that the decay predicted from the trimodal $v(\ln k)$ and the leached-fraction approximation provide an equivalent prediction of mass loss over the duration of the experiment.

Most of the quadrimodal results can also be simplified. Six of the seven data sets contain mass in two slow modes that exhibit negligible decay over the duration of the experiment. The total mass of these slow modes can therefore be equivalently represented by a constant inert mass fraction. An example of a quadrimodal distribution and its inert mass fraction approximation (located at the slowest rate in the domain) is shown in Fig. 9B. Fig. 9D shows the quadrimodal $v(\ln k)$ and its inert-mass fraction approximation predict the same decay over the duration of the experiment.

Comparing the Exit-rate Function $v(\ln k)$ to a Distribution of Rates $\rho(\ln k)$

In our previous study (Forney and Rothman 2012*a*) we identified the qualitative effects of climatic and compositional variables on the mean and variance of the nonnegative rate distribution $\rho(\ln k)$ We found that environment changes the mean, μ, of $\ln k$. Composition is correlated with both the mean and variance, σ^2, of $\ln k$ and therefore affects the faster rates of the distribution. We suggest that climatic and compositional variable may be similarly related to $v(\ln k)$. To evaluate that hypothesis, we proceed to compare the general mass-constrained exit-rate function $v(\ln k)$ to the nonnegatively constrained exit-rate function $\rho(\ln k)$.

Continuous distributions of decay rates have been used to model the degradation of organic matter (Boudreau and Ruddick 1991, Bolker et al. 1998, Rothman and Forney 2007, Manzoni et al. 2009, Feng 2009, Forney and Rothman 2012*a*). We have previously identified that the distribution associated with plant matter decay is on average lognormal (Forney and Rothman 2012*a*). Although positive rate distributions are physically consistent with a continuum of parallel first-order decays, they may also represent the exit-rate function associated with a network of possible decay states as seen above in *Example systems: Exit rates from*

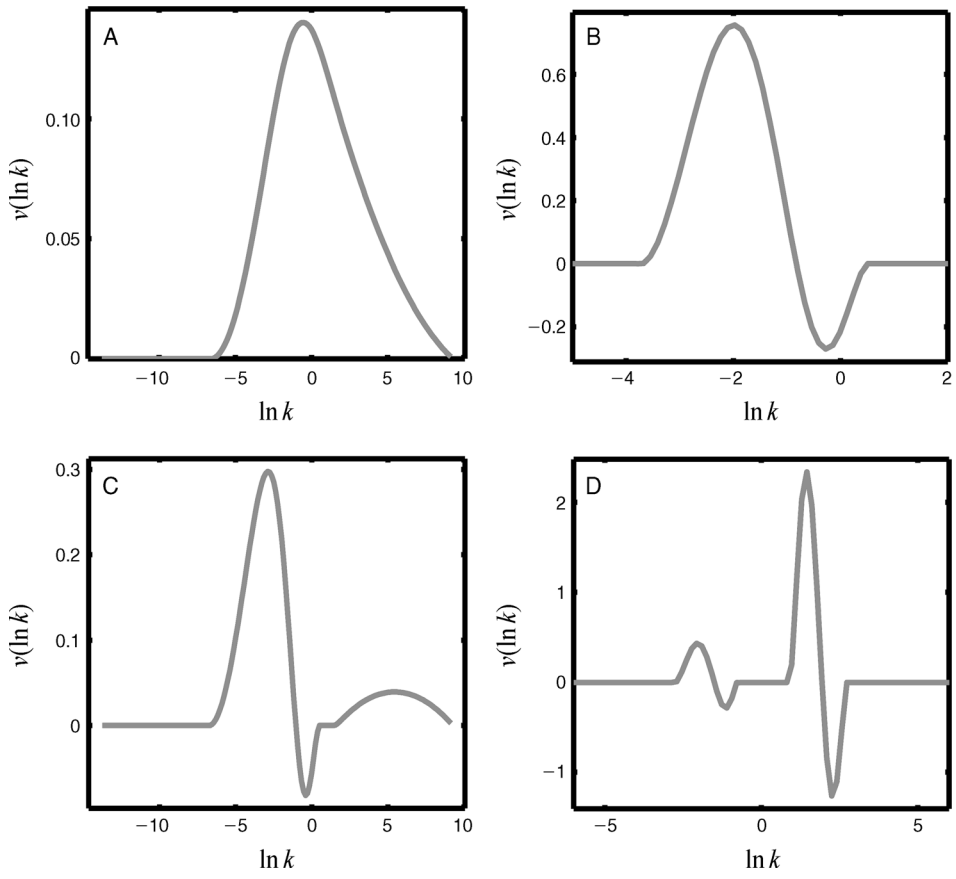

FIG. 8. Four different classes of exit-rate functions $v(\ln k)$ found among 232 LIDET data sets: (A) unimodal (38 data sets); (B) bimodal (170 data sets); (C): trimodal (12 data sets); (D): quadrimodal (7 data sets).

the CENTURY model and *Amorphous networks*. The nonnegative constraint on $\rho(\ln k)$ results in a completely monotone (essentially concave-up) decay (Forney and Rothman 2012*a*). However, the nonnegative constraint also restricts the configurations of possible decomposition networks that may best fit the data.

We find that for most LIDET data sets the distribution $\rho(\ln k)$ is typically consistent with the positive region of $v(\ln k)$ Fig. 10A shows a comparison of a typical bimodal exit-rate function to the rate distribution $\rho(\ln k)$ resulting from the nonnegative inversion associated with the data set shown in Fig. 10C. For this and a majority of the other the LIDET data sets, the negative region is typically located at fast rates and only has an effect on very early degradation times before the first measurement. The positive region explains most of the decay. Therefore a completely positive rate distribution often predicts the litterbag decay data just as well as an exit-rate function with negative components as seen in Fig. 10C. However, some data sets are more sigmoidal and exhibit a delay before decay proceeds, as shown in Fig. 10D. In this case, the negative region of the exit-rate function is spread over rates associated with the timescale of the noticeable delay, whereas the best-fitting $\rho(\ln k)$ is just a delta function at one rate (Fig. 10B). Allowing for a range of serial processes, such as decomposer community growth and sequential enzymatic activity, therefore better captures the sigmoidal shape of the decay.

In Fig. 10E we compare the root mean-square error (RMSE) of the decay predicted from $\rho(\ln k)$ and $v(\ln k)$ for 191 LIDET data sets. Fig. 10E plots the cumulative number of data sets having a RMSE less than the value shown on the horizontal axis. The general exit-rate function $v(\ln k)$, shown in red, fits the data slightly better than the positively constrained $\rho(\ln k)$ shown in blue. The mean RMSE associated with v and ρ are 0.053 and 0.056, respectively. For comparison, the mean RMSE of the best-fitting multi-pool models is 0.050, however these solutions are highly sensitive to noise (Forney and Rothman 2012*b*). The fits are similar because many of the LIDET data sets contain little to no noticeable lag time and the decay kinetics are mostly captured in the positive region of $\rho(\ln k)$. The R^2 of fitting exit-rate functions to the entire LIDET data set is 0.96; this value is high compared to other studies (Adair et al. 2008)

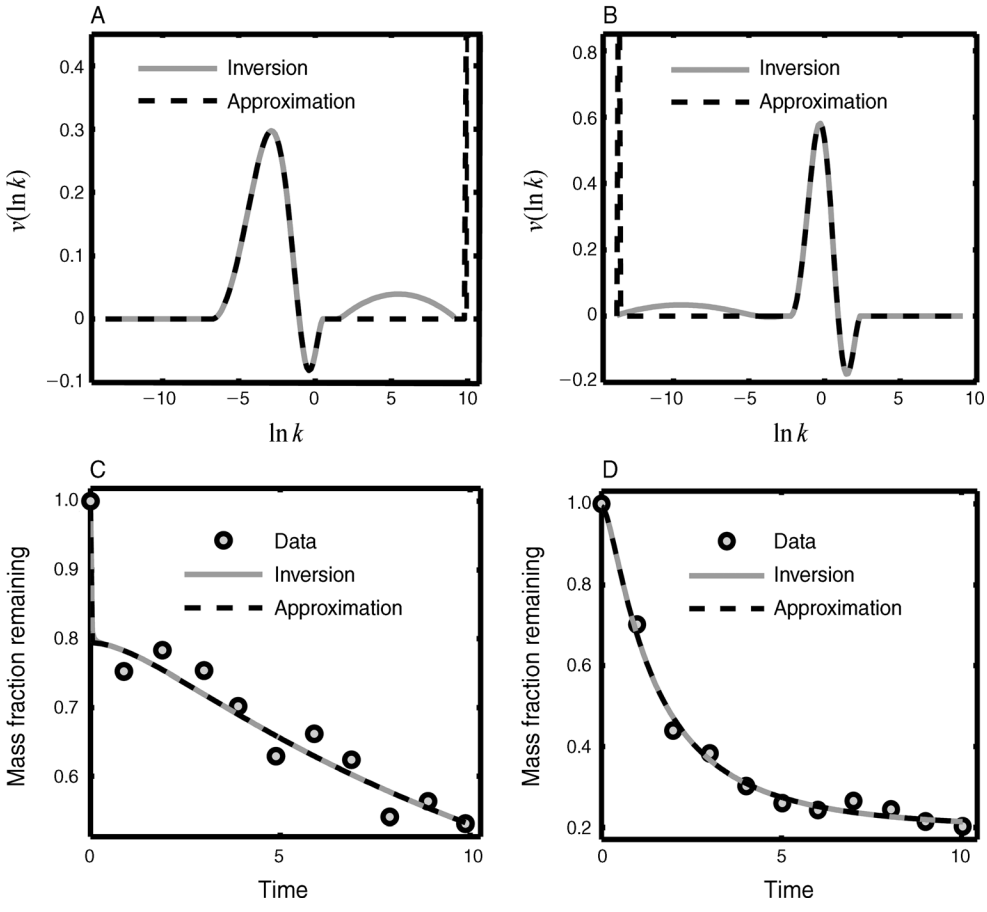

FIG. 9. Simplification of trimodal and quadrimodal data sets. (A) Example of a trimodal data set (gray) and its leached fraction approximation (dashed black). (B) Example of a quadrimodal data set (gray) and its approximation with an inert fraction (dashed black). Note the small negative mode between the two positive modes. (C) LIDET decay data (circles), predicted mass loss from the trimodal $v(\ln k)$ (gray) and the approximation (dashed black). (D) LIDET decay data (circles), predicted mass loss from the quadrimodal $v(\ln k)$ (gray) and its approximation (dashed black).

because the exit-rate functions are allowed to take arbitrary shape for each data set.

Fig. 11 compares the mean μ_ρ and variance σ_ρ of the log rate distribution $\rho(\ln k)$ to the mean μ_{v+} and standard deviation σ_{v+} of the positive portions of the exit-rate function $v(\ln k)$. Shown are the 191 LIDET data sets, which are well described by a distribution of decay rates (Forney and Rothman 2012*a*). To provide a relevant comparison to $\rho(\ln k)$ and in order to calculate a mean and variance, we rescale the positive portion of $v(\ln k)$ so that it integrates to 1. Fig. 11A shows that the means μ_ρ and μ_{v+} are highly correlated with one another. Fig. 11B also indicates that the standard deviations of the two distributions are also highly correlated. The spread in σ_{v+} at $\sigma_\rho = 0$ is associated with data sets similar to Fig. 10B; these data sets are best fit by a single rate when the exit-rate function is constrained to be nonnegative, but better fit by an exit-rate function resulting from a more general network of transformations. The additional outliers $\sigma_{v+} > \sigma_\rho$ are due to the presence of multiple positive modes in $v(\ln k)$ but not $\rho(\ln k)$.

We have previously found the distribution $\rho(\ln k)$ to be well characterized by a lognormal distribution (Forney and Rothman 2012*a*). The consistency of the calculated exit-rate function $v(\ln k)$ with the calculated rate distribution $\rho(\ln k)$ over moderate and large degradation timescales suggests that in many cases the exit rates from a degradation network can be well approximated by a lognormal distribution. Furthermore, the high correlation between μ_ρ and μ_{v+} and between σ_ρ and σ_{v+} suggests that the trends observed between climatic factors, organic matter composition, and kinetic parameters (Forney and Rothman 2012*a*) also apply to the exit rates from a decomposition network. For example, temperature and moisture appear to affect μ_ρ but not σ_ρ and thus scale all decay rates by the same factor. Therefore, because the exit rates are closely associated with the transformation rates in the decay network, we can say that climatic factors like temperature and moisture similarly affect the rates of all transformation processes. This finding

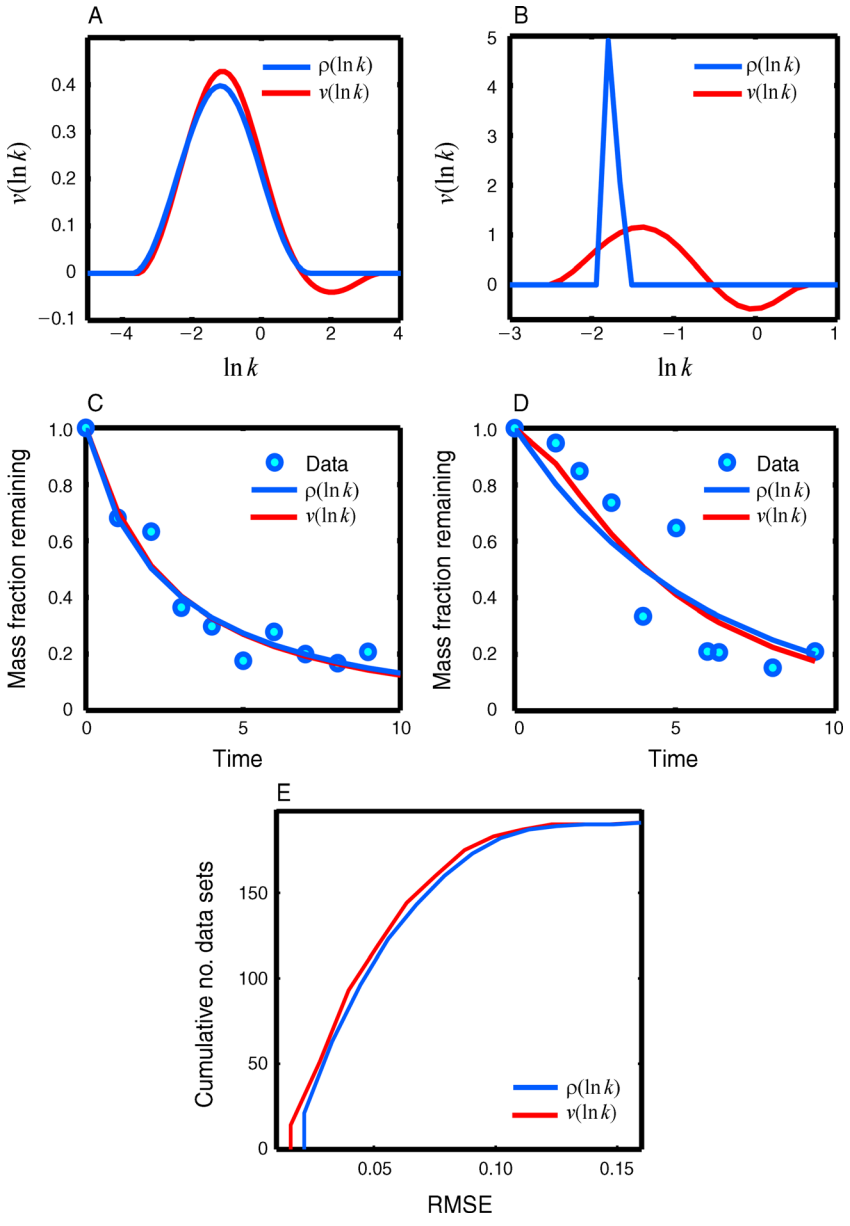

FIG. 10. Comparison of the nonnegatively constrained exit-rate function ρ(ln *k*) (Forney and Rothman 2012*a*) to the mass-loss constrained exit-rate function *v*(ln *k*). (A) Values of *v*(ln *k*) (red) and ρ(ln *k*) (blue) calculated from the inversion of the LIDET data shown in panel C. (B) Values of *v*(ln *k*) (red) and ρ(ln *k*) (blue) calculated from the inversion of the LIDET data shown in panel (D). (C) LIDET decay data (circles), predicted mass loss from *v*(ln *k*) (red) and ρ(ln *k*) (blue). (D) LIDET decay data (circles): predicted mass loss from *v*(ln *k*) (red) and (ln *k*) (blue). (E) Root mean-square error (RMSE) of the decay predicted by *v*(ln *k*) (red) and ρ(ln *k*) (blue). The vertical axis indicates the cumulative number of data sets having an RMSE less than the value shown on the horizontal axis. There are 191 data sets.

contributes to the ongoing debate regarding the temperature sensitivity of recalcitrant vs. labile organic matter decay (Davidson and Janssens 2006, Adair et al. 2008, Craine et al. 2010). Prior results (Forney and Rothman 2012*a*) also suggest that the faster pathways of the decomposition network are limited by nitrogen and sulfur and inhibited by lignin content, while more recalcitrant pathways in the network are not significantly correlated to initial organic nutrient content. In this manner, looking at the response of the exit-rate function to changes in environmental and chemical controls uncovers information regarding the underlying biological pathways. However, more rigorous methods (Adair et al. 2008, Allison 2012) are needed to parameterize the modes of the exit-rate function in terms of compositional and environmental parameters.

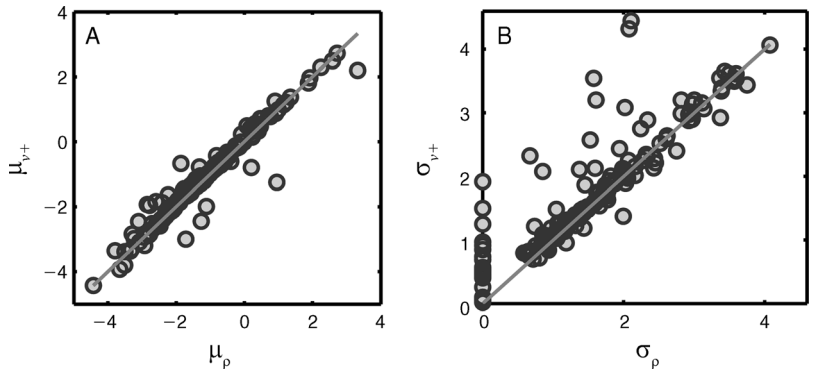

FIG. 11. Comparison of kinetic properties of the exit-rate function $v(\ln k)$ and exit-rate distribution $\rho(\ln k)$. (A) The mean log rate μ_{v+} associated with $v(\ln k)$ plotted against the mean log rate μ_ρ of the distribution $\rho(\ln k)$. (B) The standard deviation of log rates σ_{v+} associated with $v(\ln k)$ plotted against the standard deviation σ_ρ of the distribution $\rho(\ln k)$. The lines have a slope of 1 and intersect the origin. There are 191 data sets.

Discussion and Conclusions

These results suggest interpreting the continuum formulation (Eq. 22) of organic matter decay not as a distribution of components decaying in parallel, but rather as a distribution of Poisson exit rates from an underlying decay system. Carbon in any pathway of the network may react and exit at random rates. Kinetic heterogeneity associated with transformations leads to dispersion in the rates of carbon exit. This dispersion is characterized by the exit-rate function $v(\ln k)$.

The $v(\ln k)$ from the LIDET data set is consistent with a network containing two or more heterogeneous pools. More likely however, these exit-rate functions derive from a mixed continuum of states that transform at a continuum of rates. Often, carbon degradation through these complex networks are well approximated by a distribution of positive parallel rates. The presence of a negative $v(\ln k)$ indicates the existence of serial or feedback processes, while positive $v(\ln k)$ could represent parallel processes or serial and feedback processes with mass loss. In this manner, identifying $v(\ln k)$ is a coarse tool for investigating degradation network architecture. The $v(\ln k)$ obtained from litterbag studies however only characterizes the portion of the decay network associated with young soil organic matter (SOM) transformations. More work is necessary in order to probe the entire SOM network and the full domain of the exit-rate function $v(\ln k)$. Nutrient dynamics may also be included by coupling carbon kinetics to plant and microbial stoichiometry (Manzoni and Porporato 2007, Manzoni et al. 2008, Sinsabaugh and Follstad Shah 2012).

Fig. 12 summarizes the use and interpretation of the exit-rate-function approach and compares it to standard compartmental approaches for fitting and predicting decay data. Compartmental approaches require tuning the parameters associated with the compartments in order to fit decay data and predict soil organic matter dynamics. Because the exit-rate approach is an equivalent representation of linear compartmental and continuum transformation models, we advocate using the simpler exit-rate function description, $v(\ln k)$, for both system estimation and prediction of total SOM dynamics.

Conclusions

Bolker et al. (1998) have questioned the advantages of the diagonalized, eigenvalue approach over the standard forward compartmental approach in soil degradation. The exit-rate analysis via the inverse Laplace transform is a powerful tool for analyzing carbon storage and mass loss, as it accounts for particle heterogeneity and transformations, but does not require detailed information of all transformations. Thus, by describing degradation at an appropriate level of model complexity, log exit-rate function $v(\ln k)$ provides a clear visualization of the mass dynamics of the system, as well as a simple framework for analyzing the influence of biogeochemical and environmental factors on respiration.

Ultimately, the heterogeneous continuum approach here is related to the stochasticity of the various underlying nonlinear mechanisms such as enzyme kinetics (Schimel and Weintraub 2003, Moorhead and Sinsabaugh 2006, Manzoni and Porporato 2007, Allison 2012, Sinsabaugh and Follstad Shah 2012), Lotka-Volterra decomposer growth (Loreau 2001), environmental signals and cues, sorption, physical transport, and other chemical/biochemical/physical processes (Smith 1979, Manzoni and Porporato 2009). Heterogeneous continuum models assume that observed nonlinear decay dynamics result from heterogeneous transformation mechanisms with dispersed, but linear kinetics, while community based models focus on nonlinear known, but incomplete mechanisms. Both approaches include many assumptions and approximations of the true complex network of reactions responsible for degradation. Incorporating various

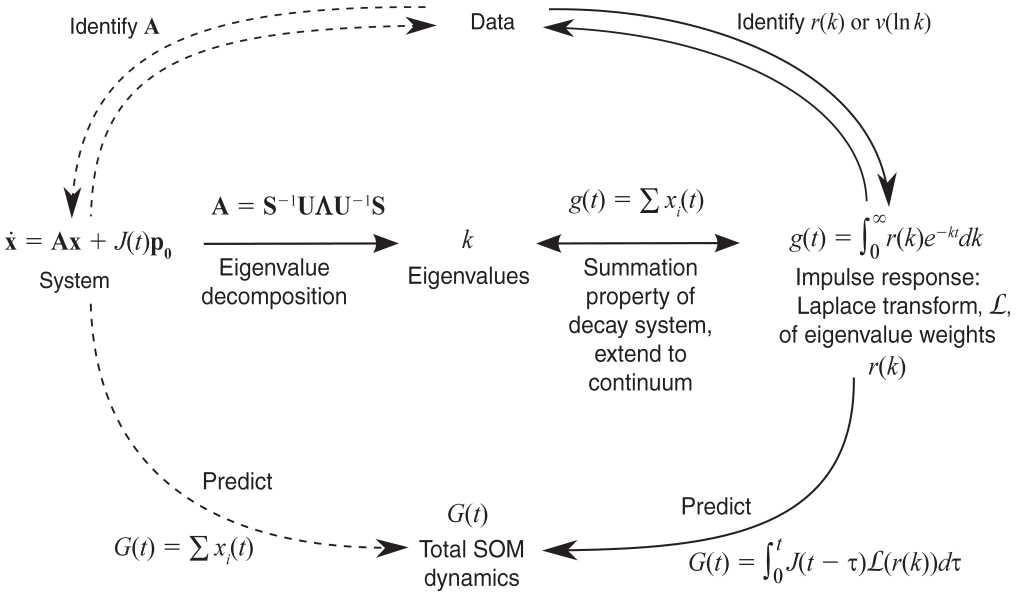

FIG. 12. Summary of the exit-rate-function approach. Standard approaches for tuning decay models are shown by the dashed lines. Full network information is necessary in the standard approach to predict soil organic matter (SOM) dynamics. By writing the impulse response of the system as $v(\ln k)$ full network information is no longer necessary. Instead only the simpler exit-rate function needs to be identified in order to predict SOM dynamics. See Table 1 for explanation of the notation.

nonlinear mechanisms into this approach will diffuse the straightforward visualization and interpretation of these first-order results, while incorporating heterogeneity/stochasticity in community-based models will further increase the complexity and uncertainty associated with an already highly parameterized approach. Both approaches may later merge together as knowledge of the underlying biology of decomposition continues to rapidly expand. On a high level, this work represents a simple approach to link—in one giant network—the metabolic pathways of the soil metagenome to the numerous decomposition pathways exterior to biological cells.

ACKNOWLEDGMENTS

We thank C. Follett, Y. Friedman, A. Petroff, H. Hartman, and O. Devauchelle for insightful discussions. This work was supported by NSF Grant EAR-0420592 and NASA Grant NNA08CN84A.

LITERATURE CITED

Adair, E. C., W. J. Parton, S. J. Del Grosso, W. L. Silver, M. E. Harmon, S. A. Hall, I. C. Burke, and S. C. Hart. 2008. Simple three-pool model accurately describes patterns of long-term litter decomposition in diverse climates. Global Change Biology 14:2636–2660.

Ågren, G. I., and E. Bosatta. 1998. Theoretical ecosystem ecology: understanding element cycles. First edition. Cambridge University Press, Cambridge, UK.

Allison, S. D. 2012. A trait-based approach for modelling microbial litter decomposition. Ecology Letters 15:1058–1070.

Allison, S., M. Weintraub, T. Gartner, and M. Waldrop. 2011. Evolutionary-economic principles as regulators of soil enzyme production and ecosystem function. Pages 229–243 *in* G. Shukla and A. Varma, editors. Soil enzymology. Volume 22 of Soil Biology. Springer-Verlag, Berlin, Germany.

Berg, B., and R. Laskowski. 2006. Litter decomposition: a guide to carbon and nutrient turnover. Elsevier, Amsterdam, The Netherlands.

Berg, B., and C. McClaugherty. 2007. Plant litter: decomposition, humus formation, carbon sequestration. Second edition. Springer-Verlag, Berlin, Germany.

Bolker, B. M., S. W. Pacala, and W. J. Parton. 1998. Linear analysis of soil decomposition: insights from the century model. Ecological Applications 8:425–439.

Bosatta, E. 1985. Theoretical analysis of decomposition of heterogeneous substrates. Soil Biology and Biochemistry 17:601–610.

Bosatta, E., and G. I. Ågren. 1991. Dynamics of carbon and nitrogen in the organic matter of the soil: a generic theory. American Naturalist 138:227–245.

Boudreau, B. P., and B. R. Ruddick. 1991. On a reactive continuum representation of organic matter diagenesis. American Journal of Science 291:507–538.

Burdige, D. J. 2006. Geochemistry of marine sediments. Princeton University Press, Princeton, New Jersey, USA.

Carpenter, S. 1981. Decay of heterogenous detritus: a general model. Journal of Theoretical Biology 89:539–547.

Carr, S. A., and R. B. Baird. 2000. Mineralization as a mechanism for TOC removal: study of ozone/ozone-peroxide oxidation using FT-IR. Water Research 34:4036–4048.

Cheng, W. 2009. Rhizosphere priming effect: Its functional relationships with microbial turnover, evapotranspiration, and C–N budgets. Soil Biology and Biochemistry 41:1795–1801.

Craine, J. M., N. Fierer, and K. K. McLauchlan. 2010. Widespread coupling between the rate and temperature sensitivity of organic matter decay. Nature Geoscience 3:854–857.

Currie, W. S., M. E. Harmon, I. C. Burke, S. C. Hart, W. J. Parton, and W. Silver. 2010. Cross-biome transplants of plant litter show decomposition models extend to a broader climatic range but lose predictability at the decadal time scale. Global Change Biology 16:1744–1761.

Cusack, D. F., W. W. Chou, W. H. Yang, M. E. Harmon, and W. L. Silver. 2009. Controls on long-term root and leaf litter decomposition in neotropical forests. Global Change Biology 15:1339–1355.

Davidson, E. A., and I. A. Janssens. 2006. Temperature sensitivity of soil carbon decomposition and feedbacks to climate change. Nature 440:165–173.

Eijsackers, H., and A. Zehnder. 1990. Litter decomposition: a Russian matriochka doll. Biogeochemistry 11:153–174.

Faddy, M. J. 1990. Compartmental models with phase-type residence-time distributions. Applied Stochastic Models in Data Analysus 6:121–127.

Faddy, M. J. 1993. A structured compartmental model for drug kinetics. Biometrics 49:243–248.

Feng, Y. 2009. K-model—a continuous model of soil organic carbon dynamics: theory. Soil Science 174:482–493.

Forney, D. C., and D. H. Rothman. 2012*a*. Common structure in the heterogeneity of plant-matter decay. Journal of the Royal Society Interface 9:2255–2267.

Forney, D. C., and D. H. Rothman. 2012*b*. Inverse method for estimating respiration rates from decay time series. Biogeosciences 9:3601–3612.

Forrester, J. W. 1961. Industrial dynamics. First edition. The M.I.T. Press, Cambridge, Massachusetts, USA.

Gangsheng, W., W. M. Post, and M. A. Mayes. 2013. Development of microbial-enzyme-mediated decomposition model parameters through steady-state and dynamic analyses. Ecological Applications 23:255–272.

Gholz, H. L., D. A. Wedin, S. M. Smitherman, M. E. Harmon, and W. J. Parton. 2000. Long-term dynamics of pine and hardwood litter in contrasting environments: toward a global model of decomposition. Global Change Biology 6:751–765.

Godfrey, K. 1983. Compartmental models and their application. Academic Press, New York, New York, USA.

Greenberg, M. 1998. Advanced engineering mathematics. Second edition. Prentice Hall, Upper Saddle River, New Jersey, USA.

Hansen, P. C. 1987. Rank-deficient and discrete ill-posed problems: numerical aspects of linear inversion. SIAM Monographs on Mathematical Modeling and Computation. Society for Industrial Mathematics, Philadelphia, Pennsylvania, USA.

Hansen, P. C. 1994. Regularization tools: a Matlab package for analysis and solution of discrete ill-posed problems. Numerical Algorithms 6:1–35.

Harmon, M. 2007. LTER intersite fine litter decomposition experiment (LIDET). Forest Science Data Bank code TD023. Oregon State University, Corvallis, Oregon, USA. http://andrewsforest.oregonstate.edu/data/abstract.cfm?dbcode=TD023

Harmon, M., and LIDET. 1995. Meeting the challenges of long-term, broad-scale ecological experiments. Publication number 19. LTER Network Office, Seattle, Washington, USA. http://intranet2.lternet.edu/documents/19-meeting-challenge-long-term-broad-scale-ecological-experiments-lidet

Harmon, M. E., W. L. Silver, B. Fasth, H. Chen, I. C. Burke, W. J. Parton, S. C. Hart, and W. S. Currie. 2009. Long-term patterns of mass loss during the decomposition of leaf and fine root litter: an intersite comparison. Global Change Biology 15:1320–1338.

Hedges, J. I., and J. M. Oades. 1997. Comparative organic geochemistries of soils and marine sediments. Organic Geochemistry 27:319–361.

Hess, M., et al. 2011. Metagenomic discovery of biomass-degrading genes and genomes from cow rumen. Science 331:463–467.

Jenkinson, D. S., S. P. S. Andrew, J. M. Lynch, M. J. Goss, and P. B. Tinker. 1990. The turnover of organic carbon and nitrogen in soil. Philosophical Transactions: Biological Sciences 329:361–368.

Kendall, D. G. 1953. Stochastic processes occurring in the theory of queues and their analysis by the method of the imbedded Markov chain. Annals of Mathematical Statistics 24:338–354.

Lamanna, R. 2005. On the inversion of multicomponent NMR relaxation and diffusion decays in heterogeneous systems. Concepts in Magnetic Resonance Part A 26A:78–90.

Lee, C., C. Arnosti, and S. Wakeham. 2004. Particulate organic matter in the sea: the composition conundrum. Ambio 33:565–575.

Liang, C., G. Cheng, D. Wixon, and T. Balser. 2010. An absorbing Markov chain approach to understanding the microbial role in soil carbon stabilization. Biogeochemistry 106:303–309.

Loreau, M. 2001. Microbial diversity, producer–decomposer interactions and ecosystem processes: a theoretical model. Proceedings of the Royal Society of London B 268:303–309.

Lützow, I. Kögel-Knabner, K. Ekschmitt, E. Matzner, G. Guggenberger, B. Marschner, and H. Flessa. 2006. Stabilization of organic matter in temperate soils: mechanisms and their relevance under different soil conditions—a review. European Journal of Soil Science 57:426–445.

Manzoni, S., R. B. Jackson, J. A. Trofymow, and A. Porporato. 2008. The global stoichiometry of litter nitrogen mineralization. Science 321:684–686.

Manzoni, S., G. G. Katul, and A. Porporato. 2009. Analysis of soil carbon transit times and age distributions using network theories. Journal of Geophysical Research 114:G04025+.

Manzoni, S., and A. Porporato. 2007. A theoretical analysis of nonlinearities and feedbacks in soil carbon and nitrogen cycles. Soil Biology and Biochemistry 39:1542–1556.

Manzoni, S., and A. Porporato. 2009. Soil carbon and nitrogen mineralization: theory and models across scales. Soil Biology and Biochemistry 41:1355–1379.

Manzoni, S., J. A. Trofymow, R. B. Jackson, and A. Porporato. 2010. Stoichiometric controls on carbon, nitrogen, and phosphorus dynamics in decomposing litter. Ecological Monographs 80:89–106.

Matis, J. H., and T. E. Wehrly. 1990. Generalized stochastic compartmental models with Erlang transit times. Journal of Pharmacokinetics and Pharmacodynamics 18:589–607.

Matis, J. H., and T. E. Wehrly. 1998. A general approach to non-Markovian compartmental models. Journal of Pharmacokinetics and Pharmacodynamics 26:437–456.

Matis, J. H., T. E. Wehrly, and W. C. Ellis. 1989. Some generalized stochastic compartment models for digesta flow. Biometrics 45:703–720.

Matis, J. H., T. E. Wehrly, and C. M. Metzler. 1983. On some stochastic formulations and related statistical moments of pharmacokinetic models. Journal of Pharmacokinetics and Pharmacodynamics 11:77–92.

Mayer, L. 1994. Relationships between mineral surfaces and organic carbon concentrations in soils and sediments. Chemical Geology 114:347–363.

Melillo, J., J. Aber, A. Linkins, A. Ricca, B. Fry, and K. Nadelhoffer. 1989. Carbon and nitrogen dynamics along the decay continuum: Plant litter to soil organic matter. Plant and Soil 115:189–198.

Minderman, G. 1968. Addition, decomposition, and accumulation of organic matter in forests. The Journal of Ecology 56:355–362.

Moorhead, D. L., and R. L. Sinsabaugh. 2006. A theoretical model of litter decay and microbial interaction. Ecological Monographs 76:151–174.

Neuts, M. F. 1995. Matrix-Geometric Solutions in Stochastic Models: An Algorithmic Approach. Revised edition. Dover Publications, Mineola, New York, USA.

Nieder, R., and D. K. Benbi. 2008. Carbon and nitrogen in the terrestrial environment. First edition. Springer-Verlag, Berlin, Germany.

Oades, J. 1988. The retention of organic matter in soils. Biogeochemistry 5:35–70.

Parton, W. J., D. S. Schimel, C. V. Cole, and D. S. Ojima. 1987. Analysis of Factors Controlling Soil Organic Matter Levels in Great Plains Grasslands. Soil Science Society of America Journal 51:1173–1179.

Parton, W. J., et al. 1993. Observations and modeling of biomass and soil organic matter dynamics for the grassland biome worldwide. Global Biogeochemical Cycles 7:785–809.

Paul, E. A. 2007. Soil microbiology, ecology and biochemistry. Third edition. Academic Press, Waltham, Massachusetts, USA.

Press, W. H., B. P. Flannery, S. A. Teukolsky, and W. T. Vetterling. 1992. Numerical recipes in C. The art of scientific computing. Second edition. Cambridge University Press, Cambridge, UK.

Rothman, D. H., and D. C. Forney. 2007. Physical model for the decay and preservation of marine organic carbon. Science 316:1325–1328.

Schimel, J. P., and M. N. Weintraub. 2003. The implications of exoenzyme activity on microbial carbon and nitrogen limitation in soil: a theoretical model. Soil Biology and Biochemistry 35:549–563.

Semple, K., K. J. Doick, K. C. Jones, P. Burauel, A. Craven, and H. Harms. 2004. Defining bioavailability and bioaccessibility of contaminated soil and sediment is complicated. Environmental Science and Technology 38:228A–231A.

Sierra, C. A., M. E. Harmon, and S. S. Perakis. 2011. Decomposition of heterogeneous organic matter and its long-term stabilization in soils. Ecological Monographs 81:619–634.

Sinsabaugh, R. L., and J. J. Follstad Shah. 2012. Ecoenzymatic stoichiometry and ecological theory. Annual Review of Ecology, Evolution, and Systematics 43:313–343.

Smith, O. L. 1979. An analytical model of the decomposition of soil organic matter. Soil Biology and Biochemistry 11:585–606.

Tenney, F. G., and S. A. Waksman. 1929. Composition of natural organic materials and their decomposition in the soil: IV. The nature and rapidity of decomposition of the various organic complexes in different plant materials, under aerobic conditions. Soil Science 28:55–84.

van Veen, J., J. Ladd, and M. Frissel. 1984. Modelling C and N turnover through the microbial biomass in soil. Plant and Soil 76:257–274.

van Veen, J. A., and E. A. Paul. 1981. Organic carbon dynamics in grassland soils. 1. Background information and computer simulation. Canadian Journal of Soil Science 61:185–201.

Vetter, Y. A., J. W. Deming, P. A. Jumars, and B. B. Krieger-Brockett. 1998. A predictive model of bacterial foraging by means of freely released extracellular enzymes. Microbial Ecology 36:75–92.

Zhou, Y., and X. Zhuang. 2006. Robust reconstruction of the rate constant distribution using the phase function method. Biophysical Journal 91:4045–4053.

Zhou, Y., and X. Zhuang. 2007. Kinetic analysis of sequential multistep reactions. Journal of Physical Chemistry B 111:13600–13610.

Supplemental Material

Appendix A

Detailed solution to the two-state example problem (*Ecological Archives* M084-006-A1).

Appendix B

Solving a linear system in order to predict mass loss from a decomposition network (*Ecological Archives* M084-006-A2).

Appendix C

Extrapolating the discrete network to the continuum (*Ecological Archives* M084-006-A3).

Appendix D

Monte Carlo method for calculating $r(k)$ from a network with heterogeneous states and distributed rates (*Ecological Archives* M084-006-A4).

Appendix E

Proof that constraints on v are sufficient to guarantee $dg/dt < 0$ (*Ecological Archives* M084-006-A5).

Supplement

MATLAB codes for the inversion algorithm and the heterogeneous CENTURY model (*Ecological Archives* M084-006-S1).

Data Availability

The LIDET data that we used for the study are publicly available in Harmon (2007): http://andrewsforest.oregonstate.edu/data/abstract.cfm?dbcode=TD023

The data were filtered for analysis by the process described in Forney and Rothman (2012*a*).